UNIVERSITA' DEGLI STUDI DI TORINO

Dipartimento di Biotecnologie Molecolari e Scienze per la Vita

Dottorato di Ricerca in Scienze Biomediche ed Oncologia

Ciclo XXIX

Anni Accademici 2014-2017

Mitotic spindle assembly and genomic stability in breast cancer require PI3K-C2α scaffolding function

Candidate: Maria Chiara De Santis

Tutor: Prof. Emilio Hirsch

PhD Coordinator: Prof. Emilio Hirsch

Alla mia famiglia

Rien ne sert de courir; il faut partir à point.
Le lièvre er la tortue, La Fontaine

Abstract

Proper organization of the mitotic spindle is key to genetic stability but molecular components of inter-microtubule bridges that crosslink kinetochore fibers (K-fibers) are still largely unknown. Here we identify a kinase-independent function of class II phosphoinositide 3-OH kinase α (PI3K-C2α) acting as limiting scaffold protein organizing clathrin and TACC3 complex crosslinking K-fibers. Downregulation of PI3K-C2α causes spindle alterations, delayed anaphase onset and aneuploidy, indicating that PI3K-C2α expression is required for genomic stability. Reduced abundance of PI3K-C2α in breast cancer models initially impairs tumor growth but later leads to the convergent evolution of fast growing clones with mitotic checkpoint defects. As a consequence of altered spindle, loss of PI3K-C2α increases sensitivity to Taxane-based therapy in preclinical models and in neoadjuvant settings. Overall, this study will open the way to more accurate patient stratification in neoadjuvant regimens.

Introduction

PI3Ks are enzymes producing 3-OH phosphorylated phosphoinositide second messengers and are involved in several processes such as proliferation, survival and metabolism (Martini et al., 2014; Vanhaesebroeck et al., 2010). PI3Ks are subdivided into three classes with PI3Kα, PI3Kβ, PI3Kδ and PI3Kγ belonging to class I, PI3K-C2α, PI3K-C2β and PI3K-C2γ to class II and Vps34 to class III. Whereas the role of class I PI3Ks in proliferation and cancer is well established, only little is known about the potential corresponding role of class II enzymes(Campa et al., 2015; Traer et al., 2006). Class II PI3Ks are large molecules ranging from 166 to 190 kDa with the PI3K catalytic core flanked by extended N- and C-terminal arms. Differently from other PI3Ks that function as heterodimers, they do not associate with adaptor proteins. Nonetheless, they participate in complex multimolecular associations through the protein and lipid binding domains contained at their N- and C-termini. For example, PI3K-C2α and PI3K-C2β can bind clathrin through their N-terminal domains and this binding is required to enhance the catalytic activity of at least PI3K-C2α (Gaidarov et al., 2001). Our recent work demonstrated that PI3K-C2α has specific non-redundant cellular functions. This enzyme is a key regulator of clathrin-mediated endocytosis (Posor et al., 2013) and of endocytic recycling required for primary cilium function (Franco et al., 2014). While these results highlight the role of PI3K-C2α in vesicular trafficking, increasing evidence is pointing to the importance of class II enzymes in cell proliferation and survival (De Santis et al., 2017; Elis et al., 2008; Franco et al., 2014; Franco et al., 2015; Gulluni et al., 2017).

Whether and how PI3K-C2α may affect cell-cycle progression and proliferation of cancer cells is still unclear. Of note, PI3K-C2α interacts with clathrin(Domin et al., 2000; Gaidarov et al., 2005), a protein that controls vesicular trafficking and mitotic spindle stability via two independent mechanisms(Royle, 2013). Whereas clathrin heavy chain (CHC) associates with the clathrin light chain (CLC) and AP1/2 adaptors on budding membranes during endocytosis, CHC finds other partners to locate at inter-MT bridges in dividing cells during metaphase. CHC is recruited to spindle by the interaction with TACC3 and its loss causes altered chromosome congression and delayed mitotic progression due to reduced kinetochore microtubule (MT) stability. PI3K-C2α strongly interacts with CHC(Domin et al., 2000; Posor et al., 2013) and this association reflects both its intracellular localization and catalytic activities(Gaidarov et al., 2005). In agreement, proteomic analysis detected PI3K-C2α in the spindle-associated clathrin-TACC3 complex (Hubner et al., 2010).

Material and Methods

Experimental model and subject details

Animals

BALB/c *Pik3c2a*$^{+/-}$ mice were previously generated (Franco et al., 2014). Mutant mice were crossed for 10 or more generations with breast cancer mouse model overexpressing the activated form of Neu oncogene (BALB/c rHER-2/NeuT) in the mammary gland(Quaglino et al., 2004). *WT/NeuT* mice were used as controls. Only individually tagged virgin female mice were used. All experiments were carried out according to the European Community guiding principles in the care and use of animals. All animal experiments were authorized by the Italian Ministry of Health (authorization number 856/2015-PR) and carried out according to the European Community guiding principles in the care and use of animals.

Human subjects

To assess the clinical relevance of PI3K-C2α expression to breast cancer, we analyzed a series of 1779 operable breast cancer patients, available on tissue microarray (TMA), who underwent surgery at the European Institute of Oncology (IEO) in Milan from years 1997 to 2000. Complete clinico-pathological and follow-up information were available for all the patients. The median length of follow-up was 14.1 years. The study was approved by the Institutional Review Board of the European Institute of Oncology (Milan, Italy) and informed consent was obtained from all subjects.

To assess the value of PI3K-C2α expression as a predictive biomarker of therapy response, we used a series of 43 breast cancer core biopsies of patients treated with Taxane-based chemotherapy in the neoadjuvant setting was retrieved from the pathology files of the Candiolo Cancer Institute IRCCS, Candiolo, Italy. Patients characteristics are available in Table S5. Pathological response on surgical specimens was categorized following (Pinder and Reis-Filho, 2007) in pathological complete response (pCR) if no residual invasive tumor was found, in situ carcinoma may be present, pathological partial response (pPR) if residual disease or minor signs of response were present on the surgical specimens compared to the tumor cellularity of the pre-treatment core biopsies, pathological non-response (pNR) if no evidence of response to therapy was detected (the presence of lymph node metastasis was not taken into account) (Balmativola et al., 2014; Pinder and Reis-Filho, 2007). With regard to the definition of molecular subtypes, we referred to the St. Gallen recommendations (Coates et al., 2015; Goldhirsch et al., 2011; Goldhirsch

et al., 2007). The study was approved by the Comittee for human Biospecimen Utilization (DSM-ChBU) of the Department of Medical Sciences, University of Turin, Italy, and informed consent was obtained from all subjects.

Cell lines and primary cultures

Tumors of different size were collected from BALB-WT/NeuT and BALB-Het/NeuT mice. Tumors were finely chopped and then digested in DMEM medium (Gibco®), containing 1 mg/ml collagenase A (Roche Applied Science, Indianapolis, IN, USA). After 30 min at 37 °C, a mixture of epithelial-enriched fragments and non-epithelial single cells was obtained. The epithelial-enriched fraction, resulting from filtration through a 70 micron mesh (BD), was digested with 0.025% trypsin-EDTA (Gibco®), centrifuged at 1200 rpm for 5 min and plated on 10-cm dish. Cells were treated with 0.025% trypsin-EDTA (Gibco®) until fibroblasts elimination and cultured in DMEM High Glucose GlutaMAXTM (Gibco®) 20% Fetal Bovine Serum (Invitrogen) supplemented with 5000 U/ml Penicillin-Streptomycin (Gibco®), 1 mM Sodium Pyruvate (Gibco®) and MEM Non-Essential Amino Acids (Gibco®). Six independent Murine Mammalian Epithelial Tumor (MMET) cells were used. Cells were detached using 0.1% trypsin-EDTA (Gibco®). Primary MEFs were obtained from E11.5 day-old embryos (Franco et al., 2014). Cells were kept in culture for no longer than 10 days, with the exception of fast-growing adapted populations of MEFs.

HeLa, HEK293T, MCF10A, MCF7, BT474, SKBR3 and T47D female cell lines were purchased from ATCC (without further authentication) and cultured in DMEM GlutaMAXTM medium supplied with 10% fetal bovine serum (FBS) and 1% Penicillin-Streptomycin (10,000 U/mL). Cell lines used in this paper are not listed in the database of commonly misidentified cell lines maintained by ICLAC. Cell lines are routinely tested for mycoplasma contamination.

Method details

Analysis of mice

To evaluate tumor appearance, all mammary glands were inspected weekly, beginning after the 8 weeks of age. The development of neoplastic lesion was performed in the fourth set of mammary glands. When tumors were detectable by palpation, neoplastic masses were measured weekly with calipers in two perpendicular diameters and the average value recorded after each examination. Tumor volume was calculated using the following formula: $d*D^2/2$, where d stands for minor diameter and D for major diameter. Progressively growing masses greater than 2 mm mean diameter were regarded as tumors. Tumors were defined "early" when $2<D<4$ mm (tumor mass no larger than 70 mm^3) and "late" when $D>6$ mm (tumor mass >100 mm^3).

Differences in tumor incidence were evaluated with Mantel-Cox log-rank test and differences in tumor multiplicity with Student's *t* test. Tumor multiplicity was calculated as the cumulative number of incident tumors per total number of mice.

For orthotopic injections, WT/NeuT and Het/NeuT MMET cells (10^6 cells) were injected in left and right fat pad of 8 weeks old *Pik3c2a*$^{+/+}$ mice. NSG mice (6-8-week-old) were injected subcutaneously (orthotopic) with 1×10^6 cells (SKBR3) or 5×10^6 MCF-7 on day 0. For MCF-7, cells were resuspended in 50% Matrigel (BD Biosciences) before sub-cutaneous injection in NSG mice. Slow release oestrogen pellets were implanted sub-cutaneously into mice two days before cell injection. About 2-4 weeks after inoculation, when the tumor reached an average volume of 70 mm^3, mice were randomized and divided into four groups (Paclitaxel, doxorubicin, combination, control). Paclitaxel (10461, Cayman Laboratories) was given 10 mg/kg, IP for 14 days (Day 1, 4, 8, 11, 14). Doxorubicin (Sigma) was given by intravenous injection each third day (six times) for 14 days at 1 mg/kg per day. The control group was treated with vehicle.

All mice were killed two weeks after the end of treatment or when the tumor mass was >1500 mm^3. Tumor masses, lymph nodes, lungs and livers were collected for histological analysis.

All experiments on mice have been performed in accordance with institutional and national guidelines and they conform to the relevant regulatory standards.

The investigators were not blinded during experiments and outcome assessment.

Histopathological analysis

For histological analysis, mammary glands were fixed overnight in 4% paraformaldehyde (PFA), embedded in paraffin and cut into 3 µm thick sections. Sections were stained with hematoxylin and eosin (H&E) following standard protocols and with specific antibodies. For protein proliferating cell nuclear antigen (PCNA, PC-10 sc-56, Santa Cruz Biotecnology) staining, slides were subjected to antigen retrieval with citrate buffer, the antibody (diluted 1:200) was localized by M.O.M kit (Vector Laboratories) and signal was detected with 3,3′-Diaminobenzidine (DAB) liquid substrate system tetrahydrochloride (Sigma-Aldrich). Slides were counterstained in eosin, dehydrated and mounted with moviol. Randomly selected areas where investigated under the light microscope (Olympus BH2), micro-photographed through digital imaging system then analyzed with ImageJ software. Apoptotic cells were detected by terminal deoxynucleotidyl transferase (TdT)-mediated dUTP nick end labeling (TUNEL) reaction (R&D Systems). Quantitative studies of immunohistochemically stained sections were performed in a blinded fashion. Sections were analyzed on an Olympus BH2 microscope (objective Olympus Plan10×), equipped with an Olympus DP50 camera for images acquisition. For murine whole-mount analysis,

fresh mammary tissue was flattened and fixed in Carnoy's solution (ethanol, glacial acetic acid, and chloroform) and subsequently stained with carmine alum (Quaglino et al., 2004).

Cell culture and proliferation

For proliferation assays via cell counts, MEFs and MMET cells were plated into 96-well plates in octuplicate at 4×10^3 cells/well and counted with a 3-(4,5-dimethyl thiazol-2-yl)-2,5-diphenyl tetrazolium bromide–based colorimetric assay (MTT) (Roche, Germany). Absorbance was recorded at days 1, 2, 3, 4, 5, 6, 7 and 8 for MEFs and days 2, 4, 6 and 8 for MMET.

For drug treatment, cells were seeded in octuplicate at 4×10^3 cells per 96-well plate; Paclitaxel and/or Doxorubicin were added the day after seeding in DMEM High Glucose GlutaMAX^{TM} (Gibco®) 5% Fetal Bovine Serum (Invitrogen) supplemented with 5000 U/ml Penicillin-Streptomycin (Gibco®), 1 mM Sodium Pyruvate (Gibco®) and MEM Non-Essential Amino Acids (Gibco®). Cells were counted 24 hours after drug treatment with a 3-(4,5-dimethyl thiazol-2-yl)-2,5-diphenyl tetrazolium bromide–based colorimetric assay (Roche, Germany). Cell survival was considered as the ratio of live cells after treatment compared with live cells treated with vehicle alone.

For MPS1 inhibition, 100 nM of NMS-P715 (475949, Calbiochem) was added the day after seeding for 48 hours.

Cell synchronization

MMET, MEF, HEK293T and HeLa cells were synchronized in metaphase using 2 mM thymidine (Sigma-Aldrich) for 20 hours, 30 µM deoxicitidine for 6 hours (Sigma-Aldrich) and 50 ng/ml of nocodazole (Sigma-Aldrich) for 12 hours, followed by 2 hours release in fresh medium in the presence of 20 µM MG132 (Calbiochem). HeLa cells were blocked in interphase by starvation for 16 hours.

Flow cytometry analysis

For DNA content determination, cells were seeded at 4×10^5 cells per 6-cm dish in triplicate. The day after seeding, cells were starved for 18 hours. Cells were detached with 0.1% trypsin-EDTA (Gibco®), fixed in ethanol 70% overnight at -20°C and stained 40 min at 37 °C with PI solution, containing 0.05% Triton X-100, 0.1 mg/ml RNase and 25 µg/ml Propidium Iodide (P4864, Sigma-Aldrich).

To determine the mitotic checkpoint status, cells were treated with 100 ng/ml nocodazole (Sigma-Aldrich) for 16 hour, followed by DNA content determination.

For Annexin V staining, cells were seeded at 4×10^5 cells per 6-cm dish in triplicate. Cells were starved 48 hours after seeding and Annexin V (556419, BD) staining was performed

according standard protocol. Sample were analyzed using a FACSCalibur flow cytometer (Becton Dickinson Immunocytometry Systems, San Jose, USA). Doublets were excluded by cell size and fluorescence intensity.

CRISPR/CAS9

For CRISPR/Cas9 mediated silencing, target sequences were designed via a gRNA design tool (Feng Lab CRISPR Design Web Tool at http://crispr.mit.edu). Each sequence was cloned into the PX335 plasmid to express the Cas9n (nickase) and two single guide RNAs (sgRNAs) were then co-trasfected in HEK293T cells to delete *PIK3C2A* gene.

Plasmids

All constructs were verified by restriction digest and automated DNA sequencing. HEK293T cells were transfected using calcium phosphate. MMET and HeLa cells were transfected by lipofection using Lipofectamine® 2000 (Life Technologies), according to the manufacturer's instructions. Doxycycline-inducible clathrin heavy chain (CHC) knockdown HeLa cells were cultured in MEM supplemented with 10% South America FBS (Euroclone), 1 mM Sodium Pyruvate (Gibco®), MEM Non-Essential Amino Acids (Gibco®), and 400 μg/ml G418 (Gibco®). HeLa cells were treated with doxycycline (0.5 μg/ml) for 7 days to achieve a >80% decrease of CHC levels.

Immunofluorescence

Immunofluorescence was performed by ice cold methanol fixation of MEF, MMET and HeLa cells followed by standard procedures(Franco et al., 2014). For PI3K-C2α staining the following protocol was used: HeLa cells were permeabilized with 0,1% Saponin for 10 seconds and then fixed in 2% PFA for 5 minutes. After two washes in PBS containing 0,1% Saponin, cells were blocked in PBS 0,1% Saponin and 2% BSA for 20 minutes. For endogenous detection of PI3K-C2α the Proteintech 22028-1-AP antibody was used at a concentration of 1:500 in blocking solution containing PBS 0,1% Saponin and 2% BSA for 1 hr. To detect the GFP- PI3K-C2α in transfected cells, anti GFP antibody (a generous gift from E. Turco)(Franco et al., 2014) was used in blocking solution for 45 minutes. Alexa secondary antibody (Alexa 488, Alexa 568 or Alexa633) were used 1:1000 for 45 minutes. Cells were stained with DAPI and examined with either Zeiss Observer-Z1 microscope, equipped with the Apotome, Leica TCS-II SP5 or Leica TSC-II SP8 confocal microscope. Raw images were digitally processed only to normalize the background and enhance the contrast. Z-stacks were acquired and processed with the Maximum Projection tool. 3D morphometric measurement and reconstruction was performed with Imaris (BitPlane, Zurich, Switzerland). To assess CHC, TACC3, PI3K-C2α and ch-TOG abundance on the spindle,

fluorescence intensity was calculated with ImageJ tools and normalized on tubulin and background fluorescence in accordance with standard methods (Burgess A et al, PNAS 2010; McCloy RA, et al Cell Cycle). At least 25 photo/genotype were taken in four independent experiments. Metaphase spindle length (the maximum distance between γ-tubulin positive spindle poles) (Fu et al., 2015), (Luo et al., 2016)and metaphase plate width (the maximum projection of DAPI positive stacks) was assessed using ImageJ distance measurement tools.

Protein analysis

Cells were homogenized in lysis buffer (120 mM NaCl, 50 mM Tris-HCl pH=8, 1% Triton X-100) supplemented with 25x protease inhibitor cocktail (Roche), 50 mM sodium fluoride and 1 mM sodium orthovanadate. Lysates were cleared by centrifugation at 13,000 rpm for 15 min at 4°C. Protein concentration was determined by Bradford method and supernatants were analyzed for immunoblotting or for immunoprecipitation (IP) with the indicated antibodies. Membranes probed with the indicated antibodies were then incubated with HRP conjugated secondary antibodies (anti-mouse used 1:10000, anti-rabbit 1:5000, Sigma) and developed with enhances chemiluminescence (ECL, BD).

For IP assays, mitotically arrested cells were used. 1 mg of pre-cleared extracts were incubated with 1 µg of the indicated antibody at 4°C on a rotating rack. After 1,5 hours, 15 µl of protein G-Sepharose (Amersham Biosciences, Buckinghamshire, UK) were added for 30 minutes. Samples were collected by centrifugation (13000 rpm 1 min) and washed six-times with lysis buffer. Bound protein complexes were then eluted by adding 30 µl Laemmli sample buffer. Spindle fractionation on HeLa and HEK293T cells was performed by incubation in a series of 4 buffers (Booth et al., 2011), followed by collection of pellets each time by centrifugation at 1000 × *g* for 4 min at room temperature and resuspension in the following buffer (Booth et al., 2011).

For pull-down experiment, HEK293T cells were transfected with GFP vector, PI3K-C2α-GFP WT or PI3K-C2α-GFP 512-670. 24 hours after transfection, cells were harvested and homogenized in lysis buffer (120 mM NaCl, 50 mM Tris-HCl pH=8, 1% Triton X-100) supplemented with 25x protease inhibitor cocktail (Roche), 50 mM sodium fluoride and 1 mM sodium orthovanadate. Lysates were cleared by centrifugation at 13,000 rpm for 15 min at 4°C. 1 mg of pre-cleared extracts were incubated with 1 µg of anti-GFP (ab1218, Abcam) and 15 µl of protein G-Sepharose for 2 hours at 4°C on a rotating rack. Samples were collected by centrifugation (13000 rpm 1 min) and washed six-times with lysis buffer. Bound protein complexes were resuspended in 500 µl of reaction buffer (50 mM Hepes pH=7.5, 100 mM NaCl, 0.05% Triton X-100, 2 mM DDT, 3 mM $MgCl_2$, protease inhibitors) and incubated with 1 µg FLAG-TACC3 (TP310754, OriGene) for 1 hour at 4°C on a rotating rack. Samples were collected by centrifugation

(13000 rpm 1 min) and washed six-times with reaction buffer. Bound protein complexes were then eluted by adding 30 µl Laemli sample buffer.

For *in vitro* binding, equimolar amount of 1 µg GST-PI3K-C2α (SRP5330, Sigma) or 140 ng GST was incubated with 15 µl of protein G-Sepharose for 30 minutes at 4°C in 500 µl of reaction buffer (50 mM Hepes pH=7.5, 100 mM NaCl, 0.05% Triton X-100, 2 mM DDT, 3 mM MgCl2, protease inhibitors), after which 1 µg FLAG-TACC3 (TP310754, OriGene) was added for 30 minutes. Beads were washed four times with 1 ml of reaction buffer and analyzed by Western blotting after the addition of 30 µl of Laemmli.

Metaphase spread preparation and Telomere-FISH (T-FISH) analysis

Cell suspensions were incubated in Colcemid (KaryoMAX Colcemid Solution; GIBCO) at the final concentration of 50 ng/mL for 3–5 hours. Metaphase spreads were prepared according to standard protocols (Franco et al., 2006). For T-FISH analysis, a FISH assay that combines DAPI staining with a Cy3-labeled telomere-specific peptide nucleic acid (PNA) probe (Cy3-[TTAGGG]3) (Applied Biosystems) was employed to assay metaphase chromosomes for instability (Franco et al., 2006). Metaphases images were acquired with BX61 Microscope (Olympus) equipped with a motorized automatic stage, a cooled-CCD camera, an interferometer (Applied Spectral Imaging), and a 633 objective lens. Analysis was performed with the HiSKY software (Applied Spectral Imaging).

Cold-treatment stability assay

HeLa cells were grown in Dulbecco's modified medium (DMEM) containing 10% FCS, 100 U/ml penicillin, 100 mg/ml streptomycin at 37°C with 5% CO_2 in a humidified incubator. Cells were transfected with PI3K-C2α siRNA or control (scramble) siRNA using lipofectamine RNAiMAX (Invitrogen) for 48 hours. Transfected cells were placed on ice and incubated in ice cold medium for 10 minutes, rinsed with cytoskeleton buffer (10 mM MES, 150 mM NaCl, 5 mM glucose, 5 mM MgCl2,) before fixing with 3% formaldehyde, 0.1% Triton X-100, and 0.1% glutaraldehyde for 15 min (Gasic et al., 2015). Cells were rinsed again with cytoskeleton buffer and stained with mouse anti-α-tubulin (1:10000, Sigma-Aldrich) and cross-adsorbed secondary antibodies (Invitrogen). To evaluate the stability of K-fibers, images of mitotic cells were collected in 2.0 µm steps using a 60x 1.4 NA objective on an inverted Nikon Eclipse Ti-E microscope equipped with a DAPI/FITC/TRYC3 filter set and a Hamamatsu Flash 4.0 SCMOS camera, and the images recorded with Nikon Imaging Software Advanced research (NIS AR).

Breast cancer patients

To assess the clinical relevance of PI3K-C2α expression to breast cancer, we analyzed a series of 1779 operable breast cancer patients, available on tissue microarray (TMA), who underwent surgery at the European Institute of Oncology (IEO) in Milan from years 1997 to 2000. Complete clinico-pathological and follow-up information were available for all the patients. The median length of follow-up was 14.1 years. The study was approved by the Institutional Review Board. Immunohistochemical staining was performed in a Bond Max Automated Immunohistochemistry Vision Biosystem (Leica Microsystems GmbH, Wetzlar, Germany) using the Bond Polymer Refine Detection Kit (DS9800). Three-µm-thick sections were prepared from formalin-fixed paraffin-embedded (FFPE) TMA tissue blocks, deparaffinized, pre-treated with the Epitope Retrieval Solution 1 (pH 6.0) at 100°C for 20 min and then incubated for 30 min with a anti-PI3K-C2α antibody (OriGene TA801690) diluted at final concentration of 1 □g/ml in Bond Primary Antibody Diluent (AR9352). TMA slides were acquired with the Aperio ScanScope system (Leica Microsystems GmbH, Wetzlar, Germany). The intensity of PI3K-C2α expression was scored from 0 to 3 (scoring categories 0, 0.5, 1, 1.5, 2, 2.5 and 3).

To assess the value of PI3K-C2α expression as a predictive biomarker of therapy response, we used a series of 43 breast cancer core biopsies of patients treated with Taxane-based chemotherapy in the neoadjuvant setting was retrieved from the pathology files of the Candiolo Cancer Institute IRCCS, Candiolo, Italy. Patients characteristics are available in Table S5. Pathological response on surgical specimens was categorized following Pinder et al.(Pinder and Reis-Filho, 2007)in pathological complete response (pCR) if no residual invasive tumor was found, *in situ* carcinoma may be present, pathological partial response (pPR) if residual disease or minor signs of response were present on the surgical specimens compared to the tumor cellularity of the pre-treatment core biopsies, pathological non-response (pNR) if no evidence of response to therapy was detected (the presence of lymph node metastasis was not taken into account) (Balmativola et al., 2014; Pinder and Reis-Filho, 2007). With regard to the definition of molecular subtypes, we referred to the St. Gallen recommendations (Coates et al., 2015; Goldhirsch et al., 2011; Goldhirsch et al., 2007). Three micron thick sections of formalin fixed paraffin embedded (FFPE) samples were stained for haematoxylin and eosin (H&E) and immunohistochemistry with antibodies against PI3K-C2α (clone OTI15H1, formerly 15H1, diluted 1:1000, Origene). Immunohistochemistry was performed using an automated slide-processing platform (Ventana BenchMarck XT Autostainer, Ventana Medical Systems). Positive and negative controls were included for each immunohistochemical run. The antibody was optimized on FFPE cell block sections of knocked down (shRNA and scramble ctrl) HeLa cells and on a series of normal tissue samples including

breast, kidney, thyroid, lymph-nodes, lung, colon. IHC scoring was based on basal staining intensities of PI3K-C2α expression in the normal breast (epithelial cells and stromal compartment) leading to a four-tier scoring system ranging from score 3 (high intensity), score 2 (moderate staining intensity, comparable to normal tissue), score 1 (reduction in staining intensity compared to normal tissue), score 0 (absence of PI3K-C2α staining with positive internal control). The study was approved by the Comittee for human Biospecimen Utilization (DSM-ChBU) of the Department of Medical Sciences, University of Turin, Italy. Patients received Paclitaxel concurrently prior to surgery as indicated as follows: doxorubicin 50 mg/m2 plus Paclitaxel 175 mg/m2 once every 3 weeks for 6 cycles, 43 patients); HER2 positive (IHC 3+ or amplified FISH) patients, in addition to the above treatment, received Trastuzumab (Herceptin) once every 3 weeks for 4 cycles.

Quantification and statistical analysis

General experimental approaches

All of the statistical details of experiments can be found in the figure legends, in the Results and the STAR Methods sections, including the statistical tests used, exact value of n, what n represents (number of animals, cells, patients, experiments) and precision measures (mean, median, SD, SEM, confidence intervals). No statistical methods were used to predetermine sample size. No samples, mice or data points were excluded from the reported analyses. Samples were not randomized to experimental groups. Sample size (number of mice) was determined on the basis of our previous studies (Franco et al., 2014; Franco et al., 2015). The investigators were not blinded to allocation during experiments and outcome assessment.

Statistical analysis

Prism software (GraphPad) was used for statistical analysis. Significance was calculated with Student t test and one- or two-way analysis of variance tests (ANOVA) followed by Bonferroni's post hoc analysis, or Mantel Cox log-rank test where appropriate. Values are reported as the mean ± standard error of the mean (SEM). For statistical analysis in breast tissue samples, we used contingency tables with Fisher's exact test or Chi square test. $p<0.05$ was considered statistically significant (*), $p<0.01$ very significant (**) and extremely significant $p<0.001$ (***).

Distant metastasis (DM) was defined as the time from surgery to the appearance of a local or regional recurrence and distant metastasis or death from breast cancer as a first event, respectively(Hudis et al., 2007). Second primary cancer or death from unknown cause or other cause were considering as competing events. For the IEO cohort, the hazard ratios (HR) of DM events in the comparison of high vs low PI3K-C2α tumors both by univariate and multivariable

analyses were estimated with Cox proportional hazards models. Multivariable models were adjusted for Grade, Ki-67, HER2 status, estrogen/progesterone status, tumor size, number of positive lymph nodes and age at surgery if available. PI3K-C2α protein status was categorized in low and high according to IHC score ≤1.0 or >1.0, respectively. Categorical data derived from (Hatzis et al., 2011; Martin et al., 2011)and IRCCS cohort were compared using chi-sq. or Fisher's exact test to estimate the effects of PI3K-C2α expression on response to neoadjuvant therapy. Agresti and Coull (modified Wald method) was used to calculate 95% confidence interval.

Gene expression data sets

We obtained raw microarray expression data for breast cancer cohorts from (Martin et al., 2011) and (Hatzis et al., 2011). Expression of PI3K-C2α was scored as "high" or "low" using the median value as threshold. Data from Table S5 are publicly available for download through the cBioPortal for Cancer Genomics (http:// http://www.cbioportal.org).

Results

Loss of PI3K-C2α impairs proliferation delaying anaphase onset

Loss of PI3K-C2α in mice causes embryonic lethality at mid-gestation due to a complex set of different phenotypes, including endothelial disorganization and primary cilium dysfunction (Franco et al., 2014; Yoshioka et al., 2012). Primary mouse embryonic fibroblasts (MEFs) derived from *Pik3c2a*$^{-/-}$ embryos displayed a strongly decreased proliferative capacity (Figure 1A) as well as increased apoptosis (Figure 1B). In line with these observations, time-lapse analysis of cell cycle in freshly isolated *Pik3c2a*$^{-/-}$ MEFs, as well as shRNA-treated HeLa cells, showed a significant delay in time required to progress from cell roundup to anaphase onset (Figure 1C and S1A-B). Next, the metaphase plate was evaluated in cells treated with 2 hours of MG132 (20 μM) to block mitotic cells in metaphase (Santaguida et al., 2011; Serio et al., 2011). Metaphase spindle length and chromosome plate width were assessed by measuring the distance between γ-tubulin positive poles and only considering aligned chromosomes (Figures 1D, 1E and S1C). Loss of PI3K-C2α resulted in altered kinetochore microtubules (MT) organization, reduced metaphase spindle length and increased chromosome plate width (Figures 1D, 1E and S1C). Heterozygous MEFs cells also displayed an intermediate phenotype, suggesting a gene dosage effect (Figures 1A-C and 1E). This revealed a so far unrecognized role of PI3K-C2α in mitosis and particularly in the chromosomal distribution occurring in metaphase. Therefore, karyotype of mutant cells was analyzed and chromosomes counts of *Pik3c2a*$^{-/-}$ MEFs displayed pronounced abnormalities (Table S1). In addition, telomere-FISH (T-FISH) analysis showed several chromatid and chromosome breaks in *Pik3c2a*$^{-/-}$ MEFs metaphase spreads (Figures 1F, 1G and Table S2). These abnormalities were consistent with disturbed cell division associated with metaphase disorganization (Castedo et al., 2004; Rieder and Maiato, 2004) and suggested, that during mitosis, loss of PI3K-C2α alters chromosome congression and segregation, eventually leading to genomic instability.

Reduction of PI3K-C2α delays tumor onset but promotes fast growing tumors

In cancer, genomic instability is a crucial driver of tumor evolution, generating phenotypic variation and adaptation under selective pressure (Hanahan and Weinberg, 2011). Thus, the impact of low levels of PI3K-C2α on cancer growth was tested by crossing *Pik3c2a*$^{+/-}$ mice with a transgenic mouse model of mammary carcinogenesis that specifically expresses the activated HER-2/Neu oncogene in the mammary gland (Quaglino et al., 2004). A cohort of *NeuT;Pik3c2a*$^{+/+}$ (WT/NeuT) and *NeuT;Pik3c2a*$^{+/-}$ (Het/NeuT) female mice was followed for about 30 weeks. WT/NeuT animals developed mammary gland tumors by 10 weeks of age with an initial tumor

latency of 8 weeks, while Het/NeuT mice showed a significantly delayed tumor latency (16 weeks; $p<0.0001$) (Figure 2A). While mammary glands of *Pik3c2a*$^{+/+}$ and *Pik3c2a*$^{+/-}$ 6/8 week-old mice appeared structurally identical, Het/Neu showed significantly less nodules than WT/Neu (Figure S2A). To evaluate hyperplastic lesions formation, mammary gland ducts of WT/NeuT and Het/NeuT 8 week-old mice were scored into four grades, according to lumen fullness (Figure S2B, left panel). In agreement with delayed onset, Het/NeuT mice developed less in situ carcinomas (Figure S2B, right panel) and showed reduced positive nuclear staining for PCNA (proliferating cell nuclear antigen) compared to control mice (Figure S2C). However, despite the delayed tumor onset, Het/NeuT mice progressively started to develop tumors that grew faster than wild-type controls (Figure 2B and Figure S2D). At sacrifice, the average number of tumors per mouse was not affected by reduction of PI3K-C2α expression. According their size, tumors were defined "early" (E) when the major diameter (D) was <4 mm and "late" (L) when D>6 mm (see *STAR Methods*).

Het/NeuT tumors expressed 50% less PI3K-C2α than controls but matching amounts of NeuT protein expression (Figure S2E), confirming that PI3K-C2α and NeuT expression were not affected by tumor size in both genotypes. Furthermore, no alteration in the AKT pathway was detected (Figure S2E). Assessment of proliferation by PCNA staining, in tumors with an average size of 150 mm^3, indicated that Het/NeuT samples display higher positivity than controls (Figure 2C). In addition, TUNEL staining revealed a higher number of apoptotic cells in E than L Het/NeuT tumors (Figures S2F and S2G). Representative images and relative quantitation of the cellularity (number of nuclei/20X-power field) of the selected images is provided in Figures S2H and S2I. These results indicate that gene dosage is key for PI3K-C2α function and that a reduction of its levels in cancer initially impairs cell proliferation but, in the long run, triggers the emergence of fast growing populations.

Reduced PI3K-C2α expression promotes genomic instability in tumor cell lines

To define the role of PI3K-C2α in the development of mammary cancer, epithelial cells were generated from primary tumors. Murine Mammary Epithelial Tumor cells (MMET) were derived from E and L, WT/NeuT and Het/NeuT tumors. Immunostaining with antibodies directed against E-cadherin confirmed the epithelial origin (Figure S2J). Early Het/NeuT MMET confirmed the *in vivo* data, showing an initial decrease in proliferation rate (Figure 2D) and a parallel increase of apoptosis (Figure S2K) followed by the invariable emergence of fast growing clones (Figure 2E).

To explore the role of PI3K-C2α in chromosomal stability, alterations in chromosome congression were analyzed during metaphase. WT/NeuT and Het/NeuT MMET were treated with 2 hours of MG132 (20 μM) to block mitotic cells in metaphase and the spindle structure was

monitored. While chromosomes aligned in a correct equatorial plane position in wild-type cells, Het/NeuT MMET displayed reduced metaphase spindle length, altered chromosome alignment and increased metaphase plate width (Figures 2F-H), in line with what observed in MEFs and HeLa cells (Figures 1D and S1C). To further validate that loss of PI3K-C2α promotes aneuploidy, cellular DNA content (ploidy) was assessed in MMET cells using Fluorescence-Activated Cell Sorting (FACS) analysis. Around 20% of both early WT/NeuT and Het/NeuT MMET showed an aberrant DNA content, likely due to the expression of NeuT, an oncogene sufficient to cause aneuploidy *per se* (Liu et al., 2002). Of note, the percentage of cells with aberrantly increased DNA content was equal in both early WT/NeuT and Het/NeuT MMET. As expected, late Het/NeuT MMET showed significantly higher aneuploidy than wild-type controls (Figure 2I). Similar results were obtained by karyotype analysis (Table S3). Taken together, these results demonstrate that PI3K-C2α controls proper metaphase spindle assembly and its loss predisposes to alteration in chromosomes congression/segregation, eventually promoting aneuploidy.

PI3K-C2α localizes on the spindle at the metaphase stage where it interacts with TACC3 and CHC

Immunofluorescence analysis of HeLa cells treated with MG132 to prevent mitotic exit revealed that PI3K-C2α is enriched along the spindle (Figures 3A and S3A). Specificity of the staining was confirmed using either a GFP-tagged PI3K-C2α (Figure 3A upper panel) or a highly specific antibody (Figures 3A, middle panel, and S3B). Furthermore, such signals disappeared from the spindle after depleting PI3K-C2α in HeLa cells (Figure 3A, lower panel). Western blot analysis also confirmed anti-PI3K-C2α immunoreactivity in mitotic spindle fractions (Figure 3B) isolated from synchronised HeLa cells (Figure S4A). Given the potential presence of PI3K-C2α in the TACC3 interactome (Hubner et al., 2010) together with the existence of a PI3K-C2α/CHC (Domin et al., 2000) and TACC3/CHC association (Cheeseman et al., 2013), interactions of PI3K-C2α in this complex were further investigated. Endogenous TACC3 and CHC co-IP with PI3K-C2α in metaphase-arrested HeLa and MMET cell lines (Figures 3C and 3D). These analyses demonstrated that, at the metaphase stage, PI3K-C2α is an integral component of the TACC3/ch-TOG/clathrin complex (Booth et al., 2011), interacting with both TACC3 and CHC. Notably, this association was not detected in interphase-arrested HeLa cells (Figure S4B). As shown in Figure 3E, PI3K-C2α–TACC3 interaction occurred preferentially on the spindle-enriched subcellular fraction, as revealed by co-IP experiments using HEK293T cells transfected with FLAG-PI3K-C2α. Subsequently, reciprocal control IP confirmed PI3K-C2α–TACC3 association in cells transfected with either TACC3-GFP (Figure S4C) or TACC3-GFP and FLAG-PI3K-C2α (Figure S4D). To further confirm

this association, direct interaction of purified proteins (Figure S4E) was assessed *in vitro*. GST-PI3K-C2α was incubated with purified TACC3 and then affinity purified together on glutathione beads, demonstrating the direct binding between PI3K-C2α and TACC3 proteins (Figure 3F). Taken together, these results revealed that PI3K-C2α is part of a protein complex which includes TACC3 and CHC.

To demonstrate that only the scaffold role of PI3K-C2α is critical for proper progression through mitosis, experiments were performed using the catalytic inactive form of PI3K-C2α [kinase dead (KD) mutant R1251P (Franco et al., 2014)] that is still able to interact with CHC but fails to rescue clathrin-mediated endocytosis (Posor et al., 2013). Co-IP experiments using either wild-type or KD PI3K-C2α demonstrated that the enzymatic function of PI3K-C2α is not required for the interaction with TACC3 (Figure S5A). Immunofluorescence analysis for phosphoinositides (Campa et al., 2015; Ciraolo et al., 2014) also revealed that neither PtdIns(3,4)P_2 nor PtdIns(3)P are located on the spindle of metaphase-arrested HeLa cells (Figure S5B).

Additionally, time lapse analysis were performed on PI3K-C2α-silenced HeLa, transfected with a siRNA-resistant version of wild-type or KD PI3K-C2α. Although the KD PI3K-C2α (Figure S5C) is not able to rescue the endocytic defect (Franco et al., 2014), both wild-type and KD PI3K-C2α completely rescued the anaphase onset delay (Figures 3G and S5D), showing that PI3K-C2α kinase activity is not required during the metaphase to anaphase transition. Taken together, these results revealed a previously unsuspected kinase-independent function of PI3K-C2α and indicate that the metaphase defect is distinct from impaired endocytosis triggered by a catalytically inactive PI3K-C2α.

To investigate which region of PI3K-C2α is required for spindle binding, a panel of ΔN-end PI3K-C2α truncation mutants was generated (Figure S5C) and their interaction with TACC3 and CHC was tested. While PI3K-C2α Δ1-380 and Δ1-512 mutants interacted with TACC3, Δ1-670 and Δ1-830 mutants were unable to bind to TACC3, delineating the region aa512-670 as the interacting surface (Figures 3H and S5E). All PI3K-C2α ΔN-end mutants failed to associate with CHC (Figures 3H and S5E), indicating that PI3K-C2α interaction with TACC3 is independent of CHC association. Next, subcellular distribution of truncated mutants was evaluated by immunofluorescence, using wild-type PI3K-C2α as control. The subcellular localization of Δ1-670 and Δ1-830 mutants was cytosolic with a diffuse pattern, while all the other isoforms were properly recruited to the spindle (Figure 3I). To conclusively demonstrate that this region is responsible for the interaction with TACC3, a GFP fusion with aa512-670 of PI3K-C2α, comprising the TACC3 binding site, was generated (GFP-PI3K-C2α512-670) (Figure S5C). This fragment was IP with anti-GFP antibodies and incubated with recombinant, FLAG-tagged TACC3. As shown in Figure S5F, the PI3K-C2α

512-670 fragment fused to GFP (but not GFP alone) was able to specifically associate with TACC3. In addition, expression of GFP-PI3K-C2α 512-670 in HeLa cells showed that this TACC3 binding fragment is sufficient to localize to the spindle independent of the binding to CHC (Figure S5G).

PI3K-C2α interacts with TACC3 and CHC to form a single complex

To investigate the sequence of events that involve PI3K-C2α in the recruitment of CHC and TACC3 at the spindle, immunofluorescence analysis of endogenous TACC3 and CHC were performed on metaphase arrested cells (Figures 4A-F, S6A-C). While spindle localization of TACC3 was unaffected by the loss of PI3K-C2α in both knockdown HeLa cells and *Pik3c2a*$^{-/-}$ MEFs (Figure 4A-C and S6A, respectively), a 75% reduction in CHC spindle levels was observed (Figure 4D-F and S6B). The decrease of CHC, but not of TACC3, from the spindle of *Pik3c2a*$^{-/-}$ MEFs (Figure S6A and S6B) and PI3K-C2α-silenced HeLa cells (Figures 4A-F), indicates that PI3K-C2α connects these two inter MT-bridges components. To fully elucidate the contribution of PI3K-C2α to the molecular network at the spindle, TACC3 expression was downregulated via siRNA in HeLa cells and the subcellular localization of PI3K-C2α and CHC was evaluated by immunofluorescence. As reported in Figures S6C and S6D, down-modulation of TACC3 reduces the spindle-associated levels of both CHC and PI3K-C2α by 78% and 70%, respectively. Lastly, to investigate if loss of PI3K-C2α affects the recruitment of ch-TOG at the spindle, immunofluorescence analysis of endogenous ch-TOG was performed on metaphase synchronized HeLa cells. As described in Figure S6E, ch-TOG spindle levels are unaffected by the reduction of PI3K-C2α, indicating that ch-TOG spindle localization is unaffected by PI3K-C2α.

Next, the effect of PI3K-C2α downregulation on TACC3/ch-TOG/clathrin complex was evaluated. A co-IP experiment was performed in mitotic arrested HEK293T cells where the expression of PI3K-C2α was disrupted using CRISPR/Cas9 technology. The loss of PI3K-C2α expression decreased the interaction between CHC-TACC3 (Figure 4G), supporting the idea that PI3K-C2α can stabilize the complex. To explore the effect of the loss of clathrin in the TACC3/ch-TOG/clathrin complex formation, HeLa cells stably expressing an inducible shRNA against CHC were used (Sorrentino et al., 2013). Formation of the TACC3/ch-TOG/clathrin complex was analyzed in cells that, after doxycycline treatment, showed >80% reduction of CHC protein. In line with a direct PI3K-C2α/TACC3 association, reduction of CHC did not affect the interaction between PI3K-C2α and TACC3 (Figure S6F).

Loss of TACC3/ch-TOG/clathrin complex is known to compromise the metaphase spindle stability due to destabilization of K-fibers (Cheeseman et al., 2013). Since tubulin acetylation and sequential detyrosination are together considered as markers of MT stability, the effects of PI3K-

C2α loss were determined by assessing the post-translational modifications of tubulin. Western blot analysis showed reduced level of the ratio between acetylated and tyrosinated tubulin in the spindle fraction of metaphase arrested MMET and PI3K-C2α-depleted HeLa cells (Figures S6G and S6H).

Reduction of PI3K-C2α caused a significant alteration of the ratio between acetylated and tyrosinated tubulin and suggested a destabilization of spindle MT. In addition, subcellular distribution of acetylated tubulin revealed a missing interaction with kinetochores in mitotically arrested PI3K-C2α-silenced HeLa cells (Figure 4H).

To test for changes in the stability of inter-MT bridges, control or PI3K-C2α-depleted HeLa cells were incubated for 10 minutes on ice, a condition known to depolymerize astral MTs (Salmon and Begg, 1980). After staining for the remaining kinetochore-MTs by immunofluorescence, spindles were classified in three categories (Amaro et al., 2010; Bird and Hyman, 2008; Gassmann et al., 2010; Vitre et al., 2014): intact mitotic spindles (category 1), partially depolymerized spindles (category 2) and severely depolymerized (category 3, Figure 4I). While control depleted cells contained over 70% of intact spindles, the typical PI3K-C2α -depleted cells with wide spindles contained only 21% intact spindles, 68% partially depolymerized spindles and 10% severely depolymerized spindles (Figure 4I). These data support the hypothesis that PI3K-C2α depletion destabilizes inter-MT bridges.

Taken together, our results demonstrate that PI3K-C2α is a member of the TACC3/ch-TOG/clathrin complex, controlling MT stability during metaphase.

PI3K-C2α deficient cells weaken mitotic checkpoint by aberrant deregulation of Spindle Assembly Checkpoint (SAC) genes

Loss of PI3K-C2α expression appears to drive aneuploidy and lead to a highly reproducible emergence of fast growing cells *in vitro* and *in vivo*. During the first two passages a reduced number of cell doubling was observed in *Pik3c2a*$^{-/-}$ MEFs but not in wild-type controls. Afterwards, a population of proliferating *Pik3c2a*$^{-/-}$ MEFs emerge, which rapidly increased and replaced the preexisting cell population (Figure S7A). This highlighted the convergent evolution of mutant cells that bypassed the requirement of PI3K-C2α in proliferation and rescued the anaphase onset delay, despite the persistence of aberrant metaphases (Figures 5A-C).

A profiling of WT/NeuT and Het/NeuT MMET (early and late stages) was performed using RealTime PCR to identify and track the expression changes of SAC genes. Late Het/NeuT tumor cells revealed recurrent abnormal expression of SAC genes, such as Cdc20 and Mad1/2 (Meraldi et al., 2004), but not of other cell cycle controllers, like cyclin B and p53 (Figures 5D and S7B-G). In addition, overexpression of Bub1 kinase was also detected (Figure S7B, S7C and S7F) but this

likely did not breach the mitotic checkpoint, as this is considered a proliferation-dependent phenomenon, correlating with the increased mitotic index (Ricke et al., 2011; van 't Veer et al., 2002). To demonstrate that inactivation of MAD genes is sufficient to overcome proliferation defects in early tumor cells, siRNA-mediated knockdown of MAD1 and MAD2 was studied in early WT/NeuT and Het/NeuT MMET. Downregulation of MAD1/2 was able to recover the proliferation defect in early Het/NeuT MMET with negligible effects in wild-type cells (Figure S7H).

To directly test for the SAC status, late WT/NeuT and Het/NeuT MMET cells were treated with low (230 nM) and high (5 μM) doses of nocodazole, a MT-interfering drug known to elicit a SAC-dependent anaphase delay (Santaguida et al., 2010) and to prevent all microtubule polymerization at the highest dose (5 μM, Figure S7I). Time-lapse analysis showed that nocodazole delayed early WT and heterozygous MMET (Table S4). The duration of mitosis in late heterozygous MMET cells was 15% or 23% shorter than in wild-type MMET, respectively, indicating a weakening of the SAC function (Figures 5E and Table S4).

To demonstrate that slow growth in early *Pik3c2a*$^{-/-}$ MEFs was due to a delayed satisfaction of the SAC, cells were treated with NMS-P715, an inhibitor of the SAC kinase Mps1 (Colombo et al., 2010; Koch et al., 2016). Administration of the drug triggered a rapid anaphase entry in mutant early MEFs (Figure 5F) and rescued their cell proliferation defect (Figure S7J), leading to a condition similar to that observed in fast growing adapted *Pik3c2a*$^{-/-}$ MEFs. In contrast, Mps1 inhibition in fast growing adapted *Pik3c2a*$^{-/-}$ MEFs did not accelerate anaphase entry, consistent with the absence of a functional SAC in these cells. Comparable results were obtained by treating with the Mps1 inhibitor early Het/NeuT MMET (Figures 5G and S7K) as well as human breast epithelial cells MCF10A carrying a CRISPR/Cas9-mediated KO of the *PIK3C2A* gene (Figures 5H and S7L). Taken together, these data demonstrate that the reduction of PI3K-C2α prevents SAC satisfaction and, in the long run, promotes the selection of fast growing clones with a weakened SAC (Figure S7M-O).

PI3K-C2α is a synthetic lethal partner of taxane-based treatments

Despite the changes in SAC strength, both early and late heterozygous MMET maintained spindle abnormalities (Figure 2F). This suggested that they could result more sensitive than wild-type controls to anti-MT drugs like Paclitaxel (Gascoigne and Taylor, 2009). As shown in Figure 6A, E and L MMET showed a significantly reduced survival when treated with doses of Paclitaxel below 100 nM and known to specifically target MT dynamics (Derry et al., 1995; Jordan et al., 1993). Re-introduction of the wild-type protein (Figure 6A) in both E and L Het/NeuT MMET cells

reduced the action of Paclitaxel without affecting the response to other chemotherapeutic agents used in breast cancer in combination with Taxanes, such as doxorubicin (Figure 6B). The increased sensitivity to Paclitaxel was also reverted in heterozygous cells rescued with KD PI3K-C2α, thus demonstrating that the catalytic activity of PI3K-C2α is not involved in this effect (Figure 6A). In addition, Paclitaxel was equally more effective in both early and late Het/NeuT cells, suggesting that only the loss of PI3K-C2α, but not of SAC function, is linked to the improved response to the drug. Similar results were obtained *in vivo* where late Het/NeuT MMET, orthotopically transplanted in syngeneic mice, displayed increased sensitivity to Paclitaxel than wild-type controls (Figure 6C). Heterozygous loss of PI3K-C2α did not enhance sensitivity to anthracyclines alone or in combination with Paclitaxel (Figure 6C).

Next, the effect of Taxol on the mitotic spindle was studied in L MMET cells. While in WT/NeuT cells treatment with Paclitaxel caused the expected 54% reduction in the number of cells with normal chromosomal alignment (Chen and Horwitz, 2002), in Het/NeuT, the same treatment, led to a 93% decrease, further confirming an additive effect on spindle microtubule stability triggered by the combination of PI3K-C2α loss and taxanes. Furthermore, the number of L Het/NeuT MMET cells with abnormal or monopolar chromosomal alignment significantly increased (Figure 6D). As a consequence of enhanced spindle abnormalities, cells that exited mitosis without division at 10 and 100 nM Paclitaxel was 65% and 54% higher in heterozygous than wild-type controls (Figure 6E and S7P). In line with these findings, L Het/NeuT MMET exiting mitosis without division generated a significantly higher number of cells with aberrant DNA content than controls (Figure 6F and S7Q). Therefore, PI3K-C2α loss and Paclitaxel additively disturb spindle microtubule structure, eventually enhancing abnormal metaphases, aneuploidy and cell death.

Role of PI3K-C2α in human breast cancer models

To assess whether changes in PI3K-C2α levels were associated with human breast cancer (BC), publicly available datasets were analyzed (Table S5). Data mining revealed that *PIK3C2A* is rarely mutated in BC (<1%) but it presents LOH in 22.8% of cases (219/960), a condition more frequent than deep deletion and/or amplification (Cerami et al., 2012; Gao et al., 2013). This pattern is specific for the *PIK3C2A* and is not shared with its closest homologue *PIK3C2B* that, in breast cancer, is more frequently amplified (12.7%) than downregulated (1%) (Table S5) (Cerami et al., 2012; Gao et al., 2013). Next, PI3K-C2α protein expression was analyzed by IHC on tissue microarrays (TMA) in a large cohort (1779 patients) of human breast cancers (Table S5). Low levels of PI3K-C2α was found in ~ 48% of the patients (IHC score ≤ 1), while ~ 52% of the patients

were classified as high expressors (IHC score > 1). This cut-off (≤1 vs. > 1, low and high respectively) was used to stratify patients with respect to indicators of disease recurrence. Stratification of individual patients for their intrinsic likelihood of developing early or late metastasis was based on the commonly used 5-year landmark (Abraham et al., 2010), which likely reflects differences in the molecular mechanisms underlying metastasis in the early and late interval (Dubsky et al., 2013). Hazard ratio (HR) was calculated with both univariate and multivariable Cox proportional hazard models with time-varying covariate. Multivariable models included grade, Ki-67, HER2 status, estrogen/progesterone status, tumor size, number of positive lymph nodes and age at surgery, if available. In the first 5 years, HR was significantly lower in patients with low PI3K-C2α but this statistically significant difference was lost in the second 5 years of followup (Table S5 and Figure S7R). Next, tumors were stratified into the three different subtypes (luminal, HER2 and basal) based on the St Gallen subtype predictor. HR was then calculated for each of the three molecular subtypes with both univariate and multivariable models. As reported in Table S5, multivariate analysis showed no statistically significant difference in HR between any of the three molecular subtypes.

To define the mechanism of this subtype-independent evolution of PI3K-C2α low breast cancers, the effect of the heterozygous loss of PI3K-C2α was evaluated in a panel of breast cancer cell lines. Given that PI3K-C2α-deficient murine cells bypass proliferative defects by deregulation of mitotic checkpoint, SAC function was tested using nocodazole-induced mitotic arrest (De Antoni et al., 2005; Kim et al., 2010; Qi and Yu, 2007). Analysis of DNA content by FACS staining showed that MCF7, but not SKBR3, cells displayed a normal SAC function and accumulated in G2/M in the presence of 100 ng/ml nocodazole. Next, MCF7 were infected with a viral vector able to silence PI3K-C2α expression. Downregulation of PI3K-C2α did not affect SAC function in MCF7 cells, as shown in FACS analysis (Figure 7A). In agreement with what observed in murine cells, shRNA-mediated downregulation of PI3K-C2α in these cells induced a strong delay in cancer growth in NSG mice (Figure 7B upper panel). Interestingly, MCF7 tumors clustered into 2 groups where growth was either completely arrested (n=6) or showed a biphasic kinetics (n=4) with an initial delay and the emergence of fast growing clones (Figure 7B, bottom panel). This was not caused by the re-expression of PI3K-C2α after shRNA-downregulation (Figure 7C) but by a spontaneous selection of clones with a weakened SAC where nocodazole was unable to trigger a G2/M arrest (Figure 7A, bottom-left panel).

To conclusively demonstrate that the evolution of tumors with reduced PI3K-C2α was caused by defects in the mitotic function of the protein, the TACC3 binding fragment of PI3K-C2α was stably expressed in SAC-proficient MCF7 cells (Figure S7S). The GFP-PI3K-C2α 512-670

mutant encompasses the amino acids that bind TACC3 but not those that bind clathrin (Figure S5F). This mutant, that lacks the bridging function of PI3K-C2α (Figure S5C), localizes on the spindle (Figure S5G) and, by definition, cannot harness other PI3K-C2α-mediated functions when expressed in the presence of the endogenous protein. Overexpression of this fragment might thus unleash a dominant negative effect, interfering with the proper assembly of the TACC3-CHC complex, but leaving the other interphase functions of the endogenous PI3K-C2α intact (ratio of internalized to surface transferrin: 1 ± 0.018 and 1.06 ± 0.07 in MCF7 transfected with GFP or GFP-PI3K-C2α 512-670 mutant, respectively). After transfection, proliferation was assessed and found to be significantly reduced (Figure S7T). To demonstrate that SAC weakening is required to overcome the defective mitotic function of PI3K-C2α, MCF7 cells stably expressing GFP-PI3K-C2α 512-670 were treated with the MPS1 inhibitor, to mimic SAC defects. As shown in Figure S7T, the proliferation impairment due to GFP-PI3K-C2α 512-670 expression was rapidly rescued after the administration of the MPS1 inhibitor. To finally demonstrate that the evolution of tumors with reduced PI3K-C2α was caused by defects in the mitotic function of the protein, MCF7 stably expressing the TACC3 binding fragment of PI3K-C2α were kept in culture for longer time. After 8 weeks of culture, 2 independent MCF7 clones expressing GFP-PI3K-C2α 512-670 emerged, that showed fast growth and SAC weakening (G2/M: 70.3 ± 1.6 and 32.2 ± 1.1, in nocodazole treated-MCF7 expressing GFP or GFP-PI3K-C2α 512-670, respectively).

This confirmed that the fragment carried a dominant negative activity unrelated to the "non mitotic" role of the PI3K-C2α enzyme. Taken together, these data further reinforced the hypothesis that, similarly to the murine model, low PI3K-C2α levels in human breast cancer models delay tumor onset only in the presence of a functional SAC while its reduction, in the long run, leads to the selection of fast growing clones with a weakened SAC.

Role of PI3K-C2α in response to Taxane-based therapy

Next, the sensitivity to Paclitaxel was assessed in a panel of human breast cancer cells in which the expression of PI3K-C2α was downregulated using shRNAs (Table S5). To exclude off-target effects due to shRNA-mediated PI3K-C2α knockdown, shRNA resistant PI3K-C2α WT or KD construct was transfected in a panel of human breast cancer cell lines (BT474, MCF7, MDA-MB231 and SKBR3) in which PI3K-C2α expression was knocked down. In all cell lines observed, sensitivity to Paclitaxel increased with loss of PI3K-C2α but returned normal in knockdown cells with the add-back of a kinase dead mutant increased (Figure 7D and Table S5). Similarly to our murine models (Figure 6B), low levels of PI3K-C2α did not affect the response to treatment with anthracyclines usually administered in combination with Taxanes (Figure 7D). Finally, increased

Paclitaxel sensitivity due to PI3K-C2α reduction was tested *in vivo* using cells with a dysfunctional SAC, such as SKBR3 (Figure 7A). As expected, downregulation of PI3K-C2α in SKBR3 cells did not change the rate of tumor growth in NSG mice but it increased sensitivity to Paclitaxel without affecting the response to the anthracycline doxorubicin (Figure 7E).

To consolidate our pre-clinical results, indicating that decreased PI3K-C2α leads to enhanced sensitivity to Paclitaxel, expression of the *PIK3C2A* gene was tested in a cohort of breast cancer patients and correlated with the response to Taxane-based neoadjuvant therapies. Given that protocols based on Taxanes alone are deprecated in neoadjuvant setting, only a very small group of patients was available (n=40). Remarkably, pathological complete response (pCR) rate was significantly higher in patients with low *PIK3C2A* (22% low *PIK3C2A* vs 4% high *PIK3C2A*, p=0.04 by chi-sq. test; Table S5). This group of patients was part of a two-arms clinical trial where 54 or 40 patients received an anthracycline-only or a Taxane-only neoadjuvant regimen, respectively (GSE21997). This allowed to test whether low *PIK3C2A* expression correlated with the response to anthracyclines. In line with our results in cell lines and xenografts, no correlation was found between low *PIK3C2A* expression and pCR to anthracyclines (n=54, 11% low *PIK3C2A* vs 11% high *PIK3C2A*, p=0.5 by chi-sq. test; Table S5). On the basis of these findings indicating that the response to anthracyclines does not depend on the expression level of *PIK3C2A*, our analysis was extended to a larger set of 4 cohorts that received a more standard combo therapy based on both anthracyclines and Taxanes. As expected from the improved response to Taxanes in low *PIK3C2A* expressors, pCR significantly correlated with low *PIK3C2A* expression (n=447, 25% low *PIK3C2A* vs 15% high *PIK3C2A*, p=0.009 by chi-sq. test; Table S5). Despite the predictive significance of ER status in breast cancer, no statistically significant difference in *PIK3C2A* level was observed in the ER positive and ER negative subgroups. Finally, to assess if findings with RNA expression could be corroborated by analysis of protein abundance, a series of pre-treatment core biopsies from 43 patients from a single-center cohort homogeneously treated with anthracyclines and Taxanes was analyzed by IHC and divided in low (score 0/1; n=12) and high (score 2/3; n=31) PI3K-C2α expressors (Figure 7F). In line with the average response to this neoadjuvant treatment (Prowell and Pazdur, 2012), the cohort showed pCR in 13.9% (6/43) of patients. No association was found between PI3K-C2α expression and ER status (Table S5). Consistent with our data *in silico*, pCR was higher in low PI3K-C2α expressors (41.7%; 95% confidence interval =19-68%) than in high PI3K-C2α expressors (3.2%; 95% confidence interval =0.0001-17%; p=0.004 by Fisher's exact test; Figure 7G and Table S5), thus indicating that low PI3K-C2α expression significantly correlates with pCR in a Taxane-based neoadjuvant chemotherapy.

Discussion

Metaphase to anaphase transition is a tightly regulated event in which quality control mechanisms ensure that all chromosomes are correctly attached to the mitotic spindle before anaphase onset. In addition to well-known metaphase players, moonlighting functions in mitosis are emerging since the discovery of the roles of clathrin at the metaphase spindle. The TACC3/ch-TOG/clathrin complex (Booth et al., 2011) is crucial for stabilizing spindle K-fibers by crosslinking adjacent microtubules (MT) (Cheeseman et al., 2013). Whether endocytosis persists during mitosis is still controversial and given the established role of PI3K-C2α in clathrin-mediated membrane trafficking, we investigated if the mitotic role of PI3K-C2α could be dependent on its endocytic function. Previous studies indicate that loss of PI3K-C2α catalytic activity blocks clathrin-coated pits maturation and CHC-mediated endocytosis (Posor et al., 2013). Accordingly, a KD PI3K-C2α mutant cannot rescue the endocytic defect that specifically depends on PI3K-C2α–mediated PtdIns(3,4)P_2 production (Posor et al., 2013). Our results showed that loss of PI3K-C2α leads to a delayed metaphase that could be fully rescued by a KD PI3K-C2α. These observations demonstrate that the role of PI3K-C2α during metaphase is independent of endocytosis but involves the association with TACC3 at the spindle. Although a direct binding between TACC3 and clathrin has been previously suggested (Hood et al., 2013), down-regulation or genetic loss of PI3K-C2α reduced the amount of CHC at the mitotic spindle. Our studies with purified proteins clearly demonstrated that PI3K-C2α directly interacts with TACC3, suggesting a tripartite complex with CHC binding both PI3K-C2α and TACC3 but where PI3K-C2α is a key stabilizer. Our findings are not in contrast with the previously identified direct interaction between TACC3 and CHC (Hood et al., 2013) but indicate that, in cultured cells, this interaction is insufficient to fully sustain the organization of the complex when the stabilizing function of PI3K-C2α is lost. In agreement with this view, in the absence of PI3K-C2α, IP of TACC3 pulls down a significantly reduced amount of CHC but does not abolish the CHC/TACC3 complex. In further agreement, the PI3K-C2α CHC-binding domain (aa1-380) and the TACC3 binding site (aa512-670) reside in two distinct regions of the protein, possibly allowing simultaneous interaction with CHC and TACC3. Moreover, our results indicated that the enrichment of PI3K-C2α at the spindle is mediated by its TACC3 binding site but is CHC-independent. We found that TACC3 spindle levels were generally unaffected by the reduction of PI3K-C2α, indicating that PI3K-C2α is not required for TACC3 spindle localization. Although the lack of CHC causes a 10% loss of TACC3 from the spindle (Booth et al., 2011), our data indicate that this small difference was likely lost due to the residual CHC/TACC3 interaction detected in PI3K-C2α knock-out cells. Overall this further corroborates the view that PI3K-C2α acts as a stabilizer of the CHC/TACC3 complex. Down-modulation of TACC3 reduced the spindle-

associated levels of both PI3K-C2α and CHC, confirming that PI3K-C2α acts downstream of TACC3 and upstream of CHC. Therefore, the impairment of inter-MT bridges, due to the loss of PI3K-C2α, results in defective K-fibers attachment and delayed mitosis.

In either early MEFs or normal breast cells (MCF10A) lacking PI3K-C2α, the delayed exit from mitosis was completely rescued by the inhibition of MPS1, a key kinase controlling SAC activation, or by MAD2 knockdown. Therefore, the disturbance in spindle organization in cells with reduced/abolished PI3K-C2α expression is sufficient to activate the SAC and delay/block metaphase completion. In line with this view, when SAC is inhibited, cells start to proliferate, thus indicating that proliferation is reduced because of SAC activation and not because of an abnormal spindle. In further agreement, spontaneously emerging fast growing clones weakened the mitotic checkpoint through the deregulation of genes responsible for sensing chromosomes binding to K-fibers, including upregulation of Cdc20 and reduced expression of the MAD genes.

While the exact role(s) of PI3K-C2α in cancer remains to be established, the sum of our results in cell culture, in experimental model systems of tumorigenesis, and in naturally occurring breast cancers argues for a complex impact of PI3K-C2α on the natural history of tumors, which possibly reflects a general physiological role of PI3K-C2α in the control of genomic stability (Hanahan and Weinberg, 2011). The biphasic dependence of tumor growth on the levels of expression of PI3K-C2α is compatible with the possibility that low levels of expression of the protein cause genomic instability, which, in turn, would initially determine an impairment in proliferative fitness but slow progress towards the emergence of aneuploidy and selection of fast growing clones. An outstanding question is whether breast cancers displaying low levels of PI3K-C2α are actual "underexpressors" and whether this is due to genetic alterations. This issue has not been directly addressed here, however, a survey of available public genomic datasets, through the cBioportal (Cerami et al., 2012; Gao et al., 2013), revealed frequent putative hemizygous deletions in the *PIK3C2A* gene in breast cancers (~23% of the cases), vis-à-vis rare mutations or putative homozygous deletions or copy gains. Notably, this alteration pattern seems specific for the *PIK3C2A* gene and it is not shared with the *PIK3C2B* gene, which is more frequently putatively amplified (20%) than downregulated in breast cancer. Thus, downregulation of *PIK3C2A* expression might randomly occur during breast cancer evolution and provide an initial detrimental effect on cell growth, later compensated by increased aneuploidy eventually leading to cancer progression.

Given the prominent role of PI3K-C2α in controlling MT stability and spindle organization, it is intriguing that a correlation between PI3K-C2α abundance and response to an anti-MT drug, like Paclitaxel, was found. Our preclinical data indicate that loss of PI3K-C2α does not influence

the response to doxorubicin, but enhances Taxol toxicity by further destabilizing kinetochore fibers. Loss of PI3K-C2α increases the number of abnormal metaphases but, in the presence of Taxol (Gascoigne and Taylor, 2009), such abnormalities are further enhanced, thus explaining the increased sensitivity detected in both SAC-proficient and -deficient cells. Mitotic checkpoint dysfunction has been previously related to resistance to Taxane-based therapy (Weaver, 2014). However, none of these reports associated a spindle dysfunction to what observed. Our study shows that increased sensitivity to Taxane-based therapies cannot be assumed for all cancers with dysfunctional SAC but that improved Taxane efficacy is a consequence of the loss of key components that, like PI3K-C2α, stabilize kinetochore fibers. In agreement with this view, enhanced Taxol sensitivity is shown by cells lacking TACC3, another component of the microtubule binding complex containing PI3K-C2α (Schmidt et al., 2010). In addition, our study associates a dysfunctional spindle to evolution towards clones with weakened SAC rather than clones that restore the lost spindle function to overcome aberrant metaphase and subsequent growth arrest. Our data thus allow to infer that increased Paclitaxel sensitivity in breast cancer is unique to the condition of reduced PI3K-C2α expression and not to the loss of SAC *per se.*

Remarkably, patients that received the neoadjuvant protocol, based on the frequent combination of Taxanes and anthracyclines, showed that reduced *PIK3C2A*/PI3K-C2α expression is associated with increased pathological complete response. Together with the finding that, in a cohort of breast cancer patients receiving anthracyclines alone, reduced *PIK3C2A* expression did not influence the clinical outcome, our results point to a specifically increased sensitivity to Taxane-based therapies in patients with low *PIK3C2A*. Anthracyclines are known to cause long-term side effects like heart failure and finding patients that can avoid this treatment is mandatory (Ghigo et al., 2016). Our findings thus suggest that the enhanced sensitivity to Taxane-based therapy associated with reduced PI3K-C2α could be exploited to stratify patients for clinical protocols with reduced side effects. In line with this view, a number of studies have explored the possibility to omit anthracyclines as a way to reduce the toxicity load for patients. Taxanes play a pivotal role in these alternative regimens, yet the exact clinical and pathological characteristics of patients who could be spared anthracyclines without compromising efficacy are currently uncertain. Therefore, our findings indicate that PI3K-C2α should be further studied in clinical trials as a potential biomarker to tailor neoadjuvant Taxane-based treatments in breast cancer patients.

Figures

Figure 1

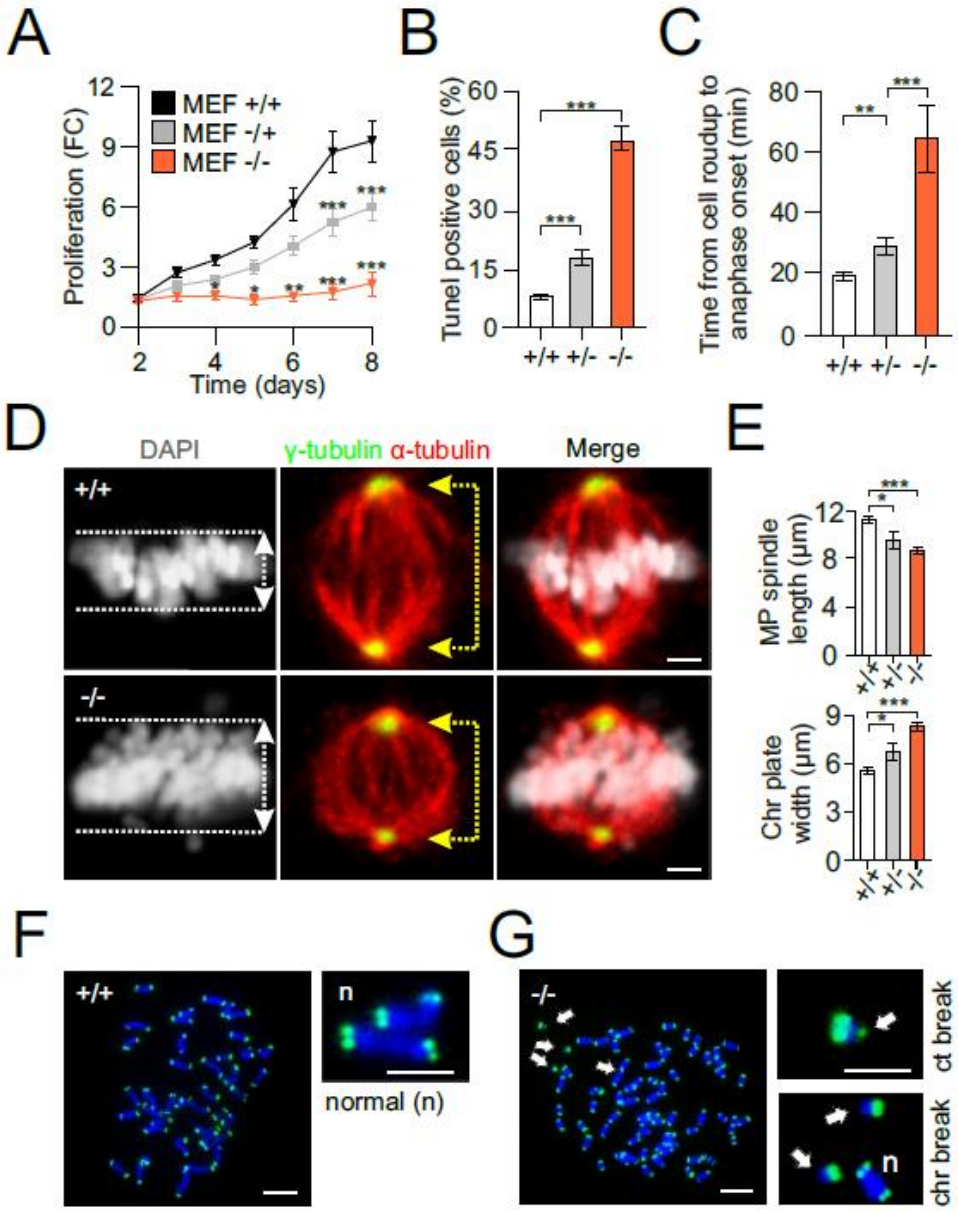

Figure 1. PI3K-C2α haploinsufficiency affects cell proliferation and induces chromosomal defects

A, Proliferation curve of freshly isolated wild–type (MEF +/+), *Pik3c2a*$^{+/-}$ (MEF +/-) and *Pik3c2a*$^{-/-}$ (MEF -/-) MEFs. FC, fold change. Results are shown as mean ± SEM (n=8). **B**, Apoptosis assay quantification (TUNEL) of freshly isolated WT, *Pik3c2a*$^{+/-}$ and *Pik3c2a*$^{-/-}$ MEFs. Results are shown as mean ± SEM (n=6). **C**, Time lapse measurement. Time required to progress from cell roundup to anaphase in freshly isolated WT, *Pik3c2a*$^{+/-}$ and *Pik3c2a*$^{-/-}$ MEFs. Results are shown as mean ± SEM (n=100 cells). **D-E**, Immunofluorescence (IF) staining of metaphase spindle length and chromosome plate width (**D**) and relative quantifications (**E**) in freshly isolated MEFs. Results are shown as mean ± SEM (n=72 cells). White arrows indicate plate width. Yellow arrows indicate spindle poles (marked by γ-tubulin). **F-G**, Representative images of telomere-FISH (T-FISH) analysis performed in whole metaphase chromosome spreads from freshly isolated +/+ (**F**) and -/- (**G**) MEFs. White arrows indicates chromosomal aberrations. Chr, chromosome; ct, chromatide; n, normal.

Unless otherwise indicated, scale bars: 5 μm; *p<0.05, **p<0.01; ***p<0.001; by analysis of variance (ANOVA) followed by Bonferroni post-hoc test.

Figure 2

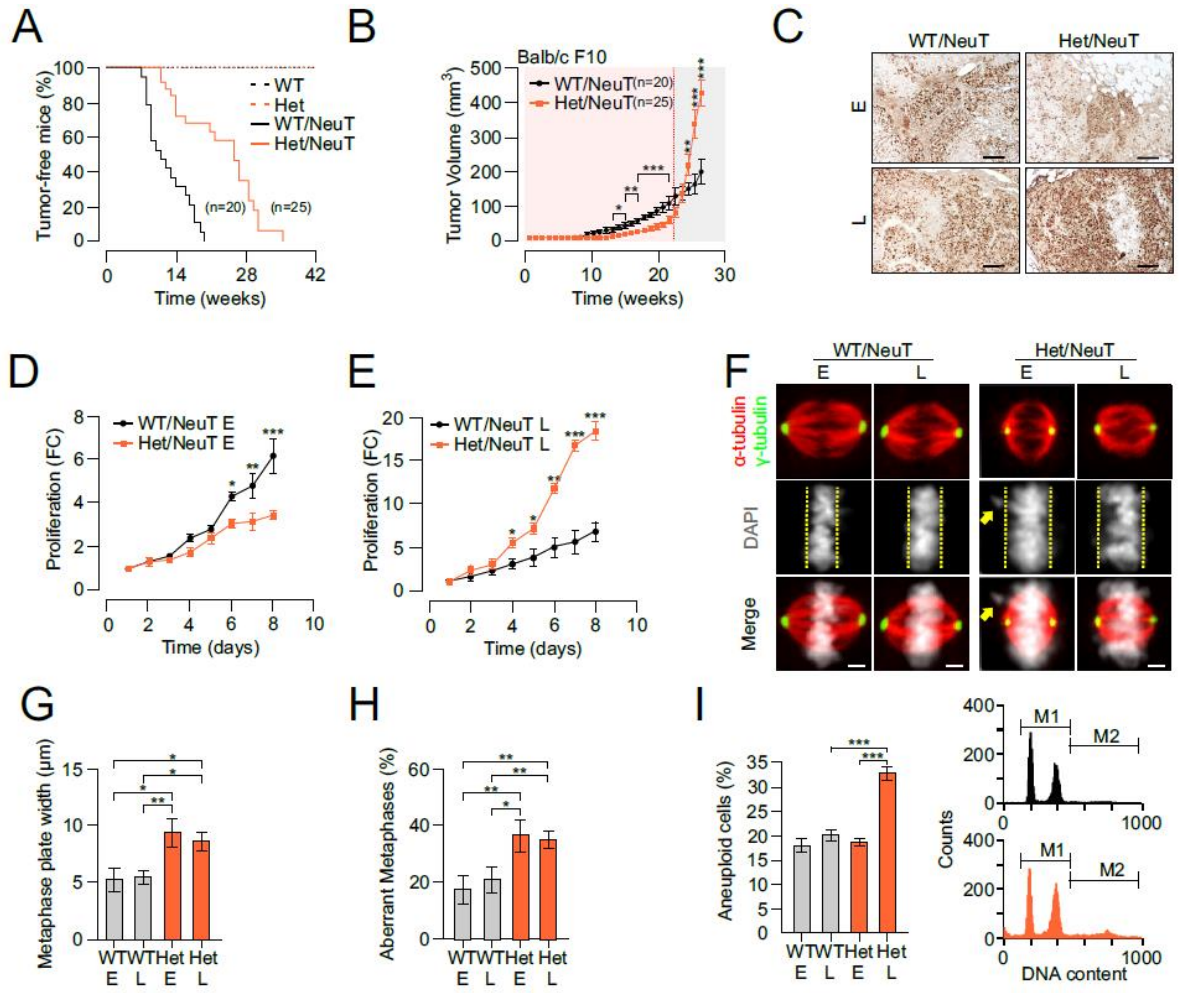
A
Tumor-free mice (%)
WT
Het
WT/NeuT
Het/NeuT
(n=20)
(n=25)
Time (weeks)
B
Balb/c F10
Tumor Volume (mm3)
WT/NeuT(n=20)
Het/NeuT(n=25)
Time (weeks)
C
WT/NeuT
Het/NeuT
E
L
D
Proliferation (FC)
WT/NeuT E
Het/NeuT E
Time (days)
E
Proliferation (FC)
WT/NeuT L
Het/NeuT L
Time (days)
F
WT/NeuT
Het/NeuT
E
L
α-tubulin
γ-tubulin
DAPI
Merge
G
Metaphase plate width (μm)
WT E
WT L
Het E
Het L
H
Aberrant Metaphases (%)
I
Aneuploid cells (%)
M1
M2
Counts
DNA content

Figure 2. PI3K-C2α haploinsufficiency affects breast cancer growth

A, Kaplan Meier curve for tumor incidence in *Pik3c2a*$^{+/+}$ (WT), *Pik3c2a*$^{+/-}$ (Het) and NeuT female mice carrying WT (WT/NeuT) or heterozygous deletion of PI3K-C2α (Het/NeuT). n=20 mice for WT/NeuT and n=25 mice for Het/NeuT. **B**, Growth curve of WT/NeuT and Het/NeuT tumors in the fourth pair of mammary glands. The red shaded background indicates the early stage of tumors while the gray one the late phase. Results are shown as mean ± SEM (n=20 mice for WT/NeuT and n=25 mice for Het/NeuT). **C**, PCNA staining of WT/NeuT and Het/NeuT tumors at early (E) or late (L) stages of development (n=6). Scale bar: 100 μm **D-E**, Proliferation curves of WT/NeuT and Het/NeuT MMET derived from E (**D**) or L (**E**) stage. FC, fold change. Results are shown as mean ± SEM (n=8). **F-H,** Analysis of metaphase plate width and aberrant metaphases. IF staining (**F**), metaphase plate width (**G**) and aberrant metaphases (**H**) quantification of E and L WT/NeuT and Het/NeuT MMET. Results are shown as mean ± SD (n=100 cells). Yellow arrows indicate lagging chromosome in metaphase. Scale bars: 5 μm. **I**, FACS analysis of E and L WT/NeuT and Het/NeuT MMET to score DNA content (PI staining). M2 gate represents the percentage of aneuploid cells. Results are shown as mean ± SEM (n=7).

Unless otherwise indicated, *p<0.05, **p<0.01; ***p<0.001; by analysis of variance (ANOVA) followed by Bonferroni post-hoc test.

Figure 3

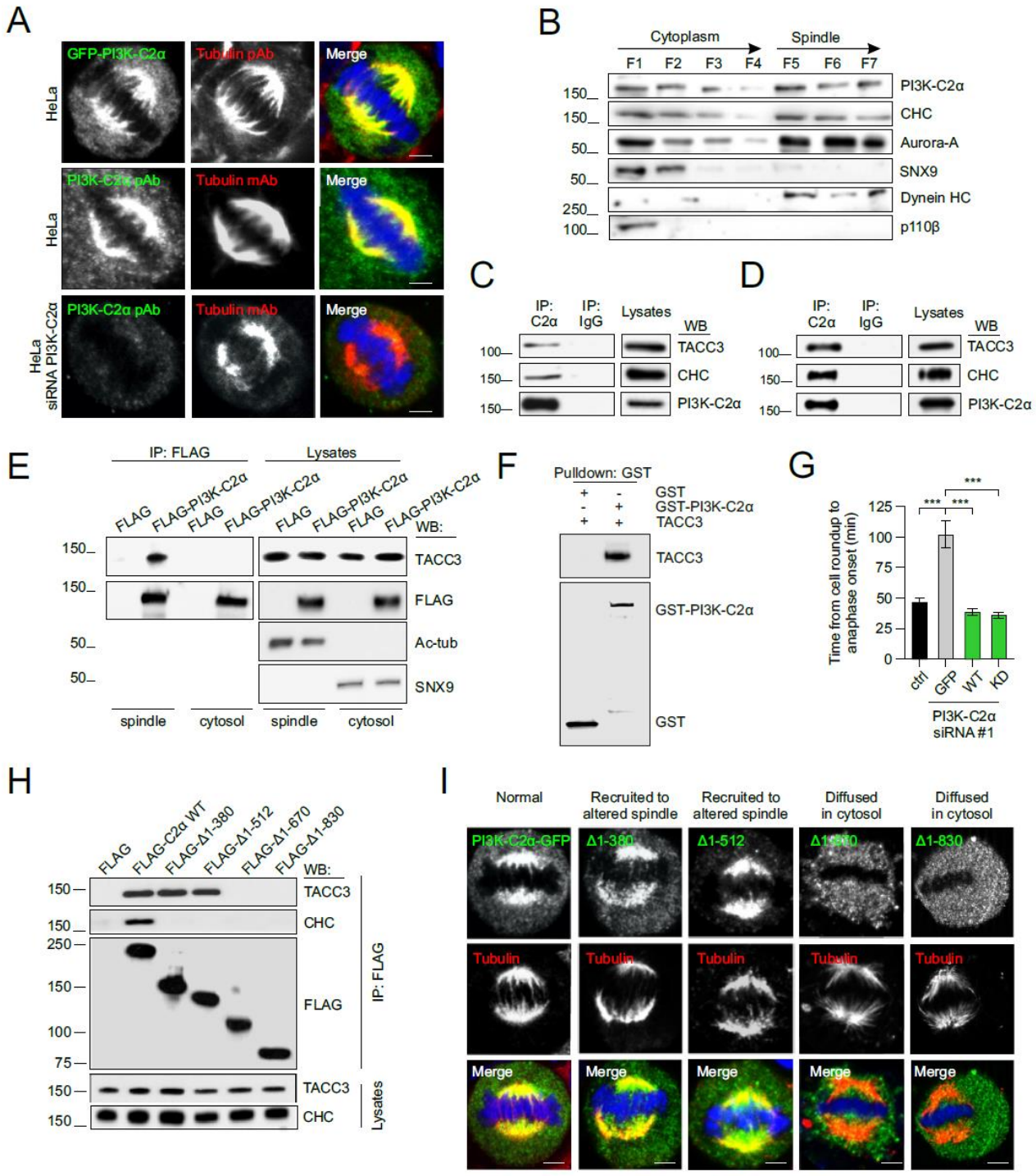
A
GFP-PI3K-C2α
Tubulin pAb
Merge
HeLa
PI3K-C2α pAb
Tubulin mAb
Merge
HeLa
PI3K-C2α pAb
Tubulin mAb
Merge
HeLa siRNA PI3K-C2α
B
Cytoplasm
Spindle
F1 F2 F3 F4 F5 F6 F7
150
150
50
50
250
100
PI3K-C2α
CHC
Aurora-A
SNX9
Dynein HC
p110β
C
IP: C2α
IP: IgG
Lysates
WB
100
150
150
TACC3
CHC
PI3K-C2α
D
IP: C2α
IP: IgG
Lysates
WB
100
150
150
TACC3
CHC
PI3K-C2α
E
IP: FLAG
Lysates
FLAG
FLAG-PI3K-C2α
FLAG
FLAG-PI3K-C2α
FLAG
FLAG-PI3K-C2α
FLAG
FLAG-PI3K-C2α
WB:
150
150
50
50
TACC3
FLAG
Ac-tub
SNX9
spindle
cytosol
spindle
cytosol
F
Pulldown: GST
+ - GST
- + GST-PI3K-C2α
+ + TACC3
TACC3
GST-PI3K-C2α
GST
G
Time from cell roundup to anaphase onset (min)
125
100
75
50
25
0
***
***
***
ctrl
GFP
WT
KD
PI3K-C2α siRNA #1
H
FLAG
FLAG-C2α WT
FLAG-Δ1-380
FLAG-Δ1-512
FLAG-Δ1-670
FLAG-Δ1-830
WB:
150
150
250
150
100
75
150
150
TACC3
CHC
FLAG
TACC3
CHC
IP: FLAG
Lysates
I
Normal
Recruited to altered spindle
Recruited to altered spindle
Diffused in cytosol
Diffused in cytosol
PI3K-C2α-GFP
Δ1-380
Δ1-512
Δ1-670
Δ1-830
Tubulin
Merge

Figure 3. PI3K-C2α localizes on metaphase spindle where it interacts with TACC3 and CHC

A, IF staining of PI3K-C2α in HeLa cells. Co-localization of exogenous (upper panel, HeLa transfected with GFP-PI3K-C2α) and endogenous PI3K-C2α (middle panel) with α-tubulin (red) on metaphase spindle. HeLa cells stained for PI3K-C2α expression after its siRNA-mediated knockdown (lower panel). **B,** WB analysis of spindle/cytoplasmic fractionation in metaphase-arrested HeLa cells. Whole cell lysates (WCL) lysates were immunoblotted with indicated antibodies (n=3). **C-D**, PI3K-C2α was IP from the cell lysate of metaphase-arrested HeLa (**C**) or MMET (**D**) with anti-PI3K-C2α antibody (IP) or control IgG. Bound proteins were detected by immunoblotting with anti-TACC3, anti-clathrin heavy chain (CHC) or anti-PI3K-C2α antibody (WB, n=6). **E**, HEK293T cells were transfected with FLAG vector or FLAG-PI3K-C2α. FLAG-PI3K-C2α was IP from cytoplasmic or spindle fraction of metaphase-arrested HEK293T cells with anti-FLAG antibody (IP). Bound proteins were detected by immunoblotting with anti-TACC3 and anti-FLAG antibody (WB). Spindle fractionation quality was assessed using anti-acetylated tubulin (spindle fraction) and anti-SNX9 (cytosol fraction) antibody (WB) (n=6). **F**, *In vitro* binding assay of equimolar amount of GST-PI3K-C2α or GST and FLAG-TACC3, using anti-GST antibody (Pulldown). Bound proteins were detected by immunoblotting with anti-TACC3 and anti-GST antibody (WB) (n=5). **G**, HeLa cells were transfected with GFP vector, siRNA resistant-GFP-PI3K-C2α or siRNA resistant-GFP- PI3K-C2α KD mutant PI3K-C2α siRNA#1 to restore the time required to pass from cell roundup to anaphase onset (control cells were transfected with scramble siRNA). Results are shown as mean ± SD (n=37 cells for wild-type and n=29 cells for KD). **H**, HEK293T cells were transfected with FLAG vector or FLAG-PI3K-C2α (WT or indicated deletion mutants). FLAG-PI3K-C2α was IP in metaphase-arrested HEK293T cells with anti-FLAG antibody (IP). Bound proteins were blotted with anti-TACC3, anti-CHC or anti-FLAG antibody (WB) (n=6). **I**, IF staining of PI3K-C2α (wild-type or indicated deletion mutants) in metaphase-arrested HeLa cells (n=3). HeLa cells were transfected with GFP-PI3K-C2α (wild-type or indicated mutants) and co-localization with α-tubulin (red) on metaphase spindle was evaluated.

Unless otherwise indicated, scale bars: 5 μm; *p<0.05, **p<0.01; ***p<0.001; by analysis of variance (ANOVA) followed by Bonferroni post-hoc test.

Figure 4

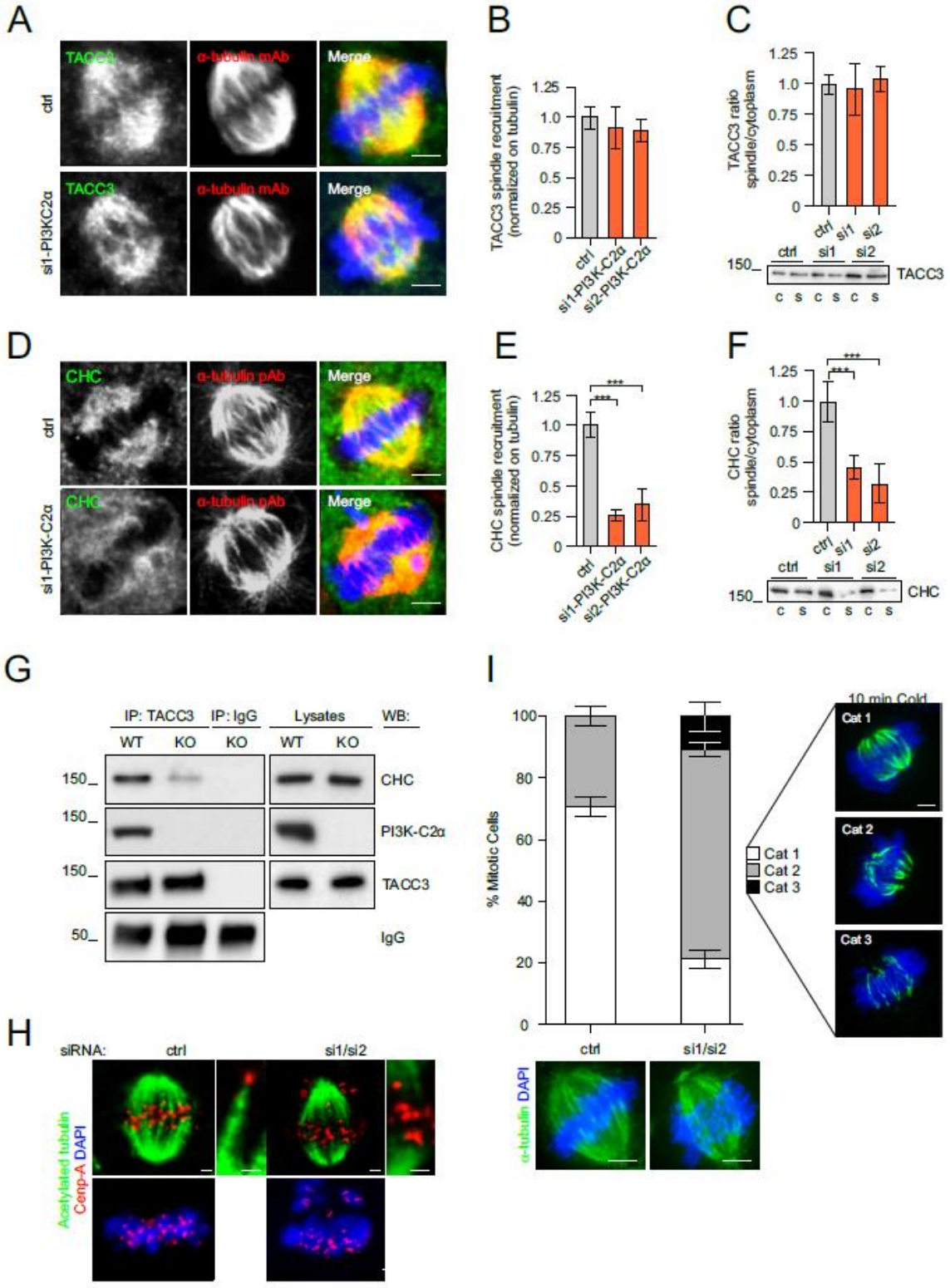
A
TACC3
α-tubulin mAb
Merge
ctrl
si1-PI3KC2α
B
TACC3 spindle recruitment (normalized on tubulin)
ctrl
si1-PI3K-C2α
si2-PI3K-C2α
C
TACC3 ratio spindle/cytoplasm
ctrl
si1
si2
150_
TACC3
c s c s c s
D
CHC
α-tubulin pAb
Merge
si1-PI3K-C2α
E
CHC spindle recruitment (normalized on tubulin)
***
F
CHC ratio spindle/cytoplasm
CHC
G
IP: TACC3
IP: IgG
Lysates
WB:
WT
KO
KO
WT
KO
150_
CHC
PI3K-C2α
TACC3
50_
IgG
H
siRNA:
ctrl
si1/si2
Acetylated tubulin
Cenp-A DAPI
I
10 min Cold
% Mitotic Cells
Cat 1
Cat 2
Cat 3
α-tubulin DAPI

Figure 4. PI3K-C2α organizes the mitotic spindle by stabilizing the TACC3-CHC complex

A-C, Analysis of TACC3 localization. IF staining (**A**), relative quantification (**B**) and WB analysis (**C**) of TACC3 localization on metaphase spindle and cytosolic fraction in control and PI3K-C2α-silenced HeLa cells. Results are shown as mean ± SEM (IF n=200 cells; WB n=5). **D-F**, Analysis of CHC localization. IF staining (**D**), relative quantification (**E**) and WB analysis (**F**) of CHC localization on metaphase spindle and cytosolic fraction of wild-type and PI3K-C2α-silenced HeLa cells. Results are shown as mean ± SEM (IF n=200 cells; WB n=5). **G**, HEK293T were transfected with CRISPR/Cas9 KO plasmid targeting *PIK3C2A* gene (KO). After clone isolation, TACC3 was IP with anti-TACC3 antibody (IP). Bound proteins were blotted with anti-CHC, anti-TACC3 or anti-PI3K-C2α antibody (WB) (n=6). **H**, IF staining of acetylated tubulin (green), Cenp-A (red) and DAPI (blue) in ctrl and PI3K-C2α -silenced HeLa cells (n=3). **I**, Quantification of kinetochore-MT stability. Stacked bar graph indicates the percentage of the 3 different morphological categories exemplified on the right in control or PI3K-C2α-depleted HeLa cells. Results are shown as mean ± SEM of calculated % (n=47 cells).

Unless otherwise indicated, scale bars: 5 μm; *p<0.05, **p<0.01; ***p<0.001; by analysis of variance (ANOVA) followed by Bonferroni post-hoc test.

Figure 5

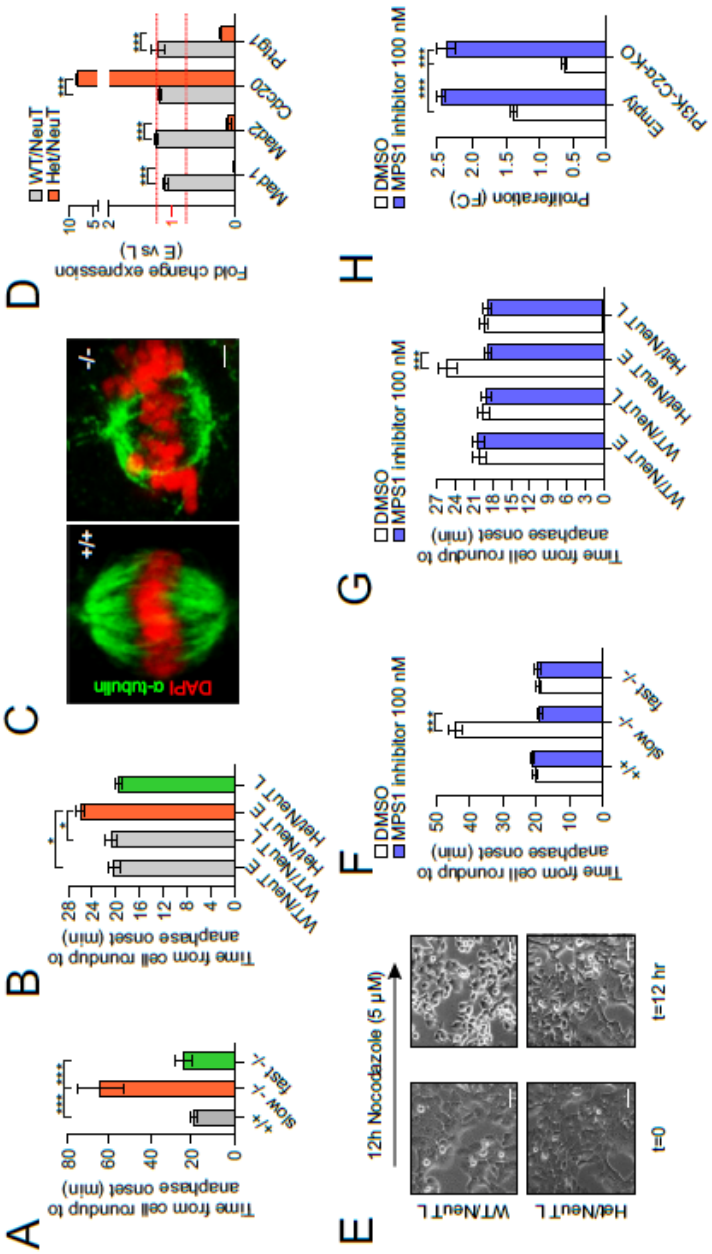
A
Time from cell roundup to anaphase onset (min)
+/+
slow -/-
fast -/-
B
Time from cell roundup to anaphase onset (min)
WT/NeuT L
WT/NeuT E
Het/NeuT L
Het/NeuT E
C
DAPI α-tubulin
+/+
-/-
D
Fold change expression (E vs L)
WT/NeuT
Het/NeuT
Mad1
Mad2
Cdc20
Plk1
E
12h Nocodazole (5 μM)
t=0
t=12 hr
WT/NeuT L
Het/NeuT L
F
DMSO
MPS1 inhibitor 100 nM
Time from cell roundup to anaphase onset (min)
+/+
slow -/-
fast -/-
G
DMSO
MPS1 inhibitor 100 nM
Time from cell roundup to anaphase onset (min)
WT/NeuT E
WT/NeuT L
Het/NeuT E
Het/NeuT L
H
DMSO
MPS1 inhibitor 100 nM
Proliferation (FC)
Empty
PI3K-C2α-KO

Figure 5. Candidate genes of the SAC bypass metaphase defect in PI3K-C2α deficient cells.

A-B, Time required to progress from cell roundup to anaphase in wild-type, early and fast growing adapted *Pik3c2a*$^{-/-}$ MEFs (**A**) and MMET cells (**B**). Results are shown as mean ± SD (n=100 cells). **C**, IF staining of wild-type and fast growing adapted *Pik3c2a*$^{-/-}$ MEFs metaphases (n=5). Scale bars: 5 μm. **D**, Quantitative Real Time PCR analysis of expression of SAC-related genes in MMET cells. Results are shown as mean ± SD (n=5). **E**, Representative images of late, fast growing WT and Het/NeuT MMET cells treated with 5 μM nocodazole for 12 hr. Scale bars: 60 μm. **F-G**, Effect of spindle assembly checkpoint kinase MPS1 (MPSi) inhibitor on the time required to progress from cell roundup to anaphase on wild-type and *Pik3c2a*$^{-/-}$ MEFs (**F**) and MMET (**G**). Results are shown as mean ± SEM (n=200 cells). **H**, Effect of spindle assembly checkpoint kinase MPS1 (MPSi) inhibitor on MCF10A after *PIK3C2A* CRISPR/Cas9-targeted deletion. Data are normalized on untreated empty MCF10A cells after 48 hours. Results are shown as mean ± SEM (n=5).

Unless otherwise indicated, *p<0.05, **p<0.01; ***p<0.001; by analysis of variance (ANOVA) followed by Bonferroni post hoc test.

Figure 6

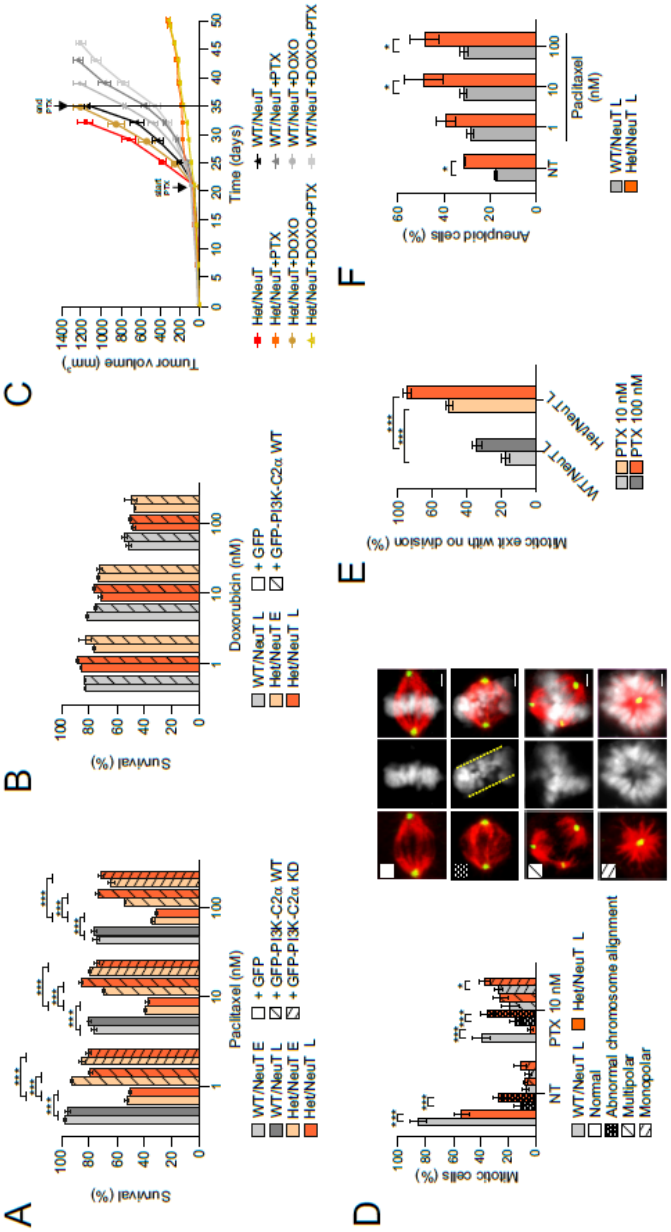
A
Survival (%)
Paclitaxel (nM)
WT/NeuT E
WT/NeuT L
Het/NeuT E
Het/NeuT L
+ GFP
+ GFP-PI3K-C2α WT
+ GFP-PI3K-C2α KD
B
Survival (%)
Doxorubicin (nM)
WT/NeuT L
Het/NeuT E
Het/NeuT L
+ GFP
+ GFP-PI3K-C2α WT
C
Tumor volume (mm³)
Time (days)
start PTX
end PTX
Het/NeuT
Het/NeuT+PTX
Het/NeuT+DOXO
Het/NeuT+DOXO+PTX
WT/NeuT
WT/NeuT+PTX
WT/NeuT+DOXO
WT/NeuT+DOXO+PTX
D
Mitotic cells (%)
NT
PTX 10 nM
WT/NeuT L
Het/NeuT L
Normal
Abnormal chromosome alignment
Multipolar
Monopolar
E
Mitotic exit with no division (%)
WT/NeuT L
Het/NeuT L
PTX 10 nM
PTX 100 nM
F
Aneuploid cells (%)
NT
Paclitaxel (nM)
WT/NeuT L
Het/NeuT L

Figure 6. PI3K-C2α is a synthetic lethality partner of Taxane-based treatment

A, Effect of Paclitaxel (PTX) anti-proliferative activity, measured as % cell survival after treatment, on WT/NeuT and Het/NeuT MMET (plain bars) and rescue experiments with wild-type or KD PI3K-C2α (dashed bars). Results are shown as mean ± SD (n=5). **B,** Effect of Doxorubicin (DOXO) anti-proliferative activity, measured as % cell survival after treatment, on WT/NeuT and Het/NeuT MMET (plain bars) and rescue experiments with wild-type or KD PI3K-C2α (dashed bars) to restore resistance to DOXO treatment. Results are shown as mean ± SD (n=5). **C**, Effect of PTX, DOXO or combination of the two drugs (PTX+DOXO) on orthotopic MMET tumors engrafted in syngeneic mice. The treatment was started after 20 days from tumor inoculation (start PTX) and was stopped 15 days later (end PTX). Tumor volume is shown as mean ± SEM (n=6 mice). **D**, IF analysis of mitotic spindles in WT/NeuT L and Het/NeuT L treated with 10 nM of PTX or vehicle only. Spindles where subdivided in four categories (normal, abnormal chromosome alignment, multipolar and monopolar) and percentage of each category was reported in the graph. Results are shown as mean ± SD (n=80). Scale bars: 5 μm. **E**, Time lapse analysis of late WT/NeuT and Het/NeuT treated with 10 nM or 100 nM of PTX or vehicle only. Percentage of cells exiting mitosis with no division was reported in graph. Results are shown as mean ± SD (n=100). **F**, FACS analysis of late WT/NeuT and Het/NeuT MMET to score DNA content (PI staining) after treatment with PTX (indicated dosage, 24 hr). Percent of cells with aneuploidy are shown as mean ± SEM (n=5).
Unless otherwise indicated, *p<0.05, **p<0.01; ***p<0.001; by analysis of variance (ANOVA) followed by Bonferroni post-hoc test.

Figure 7

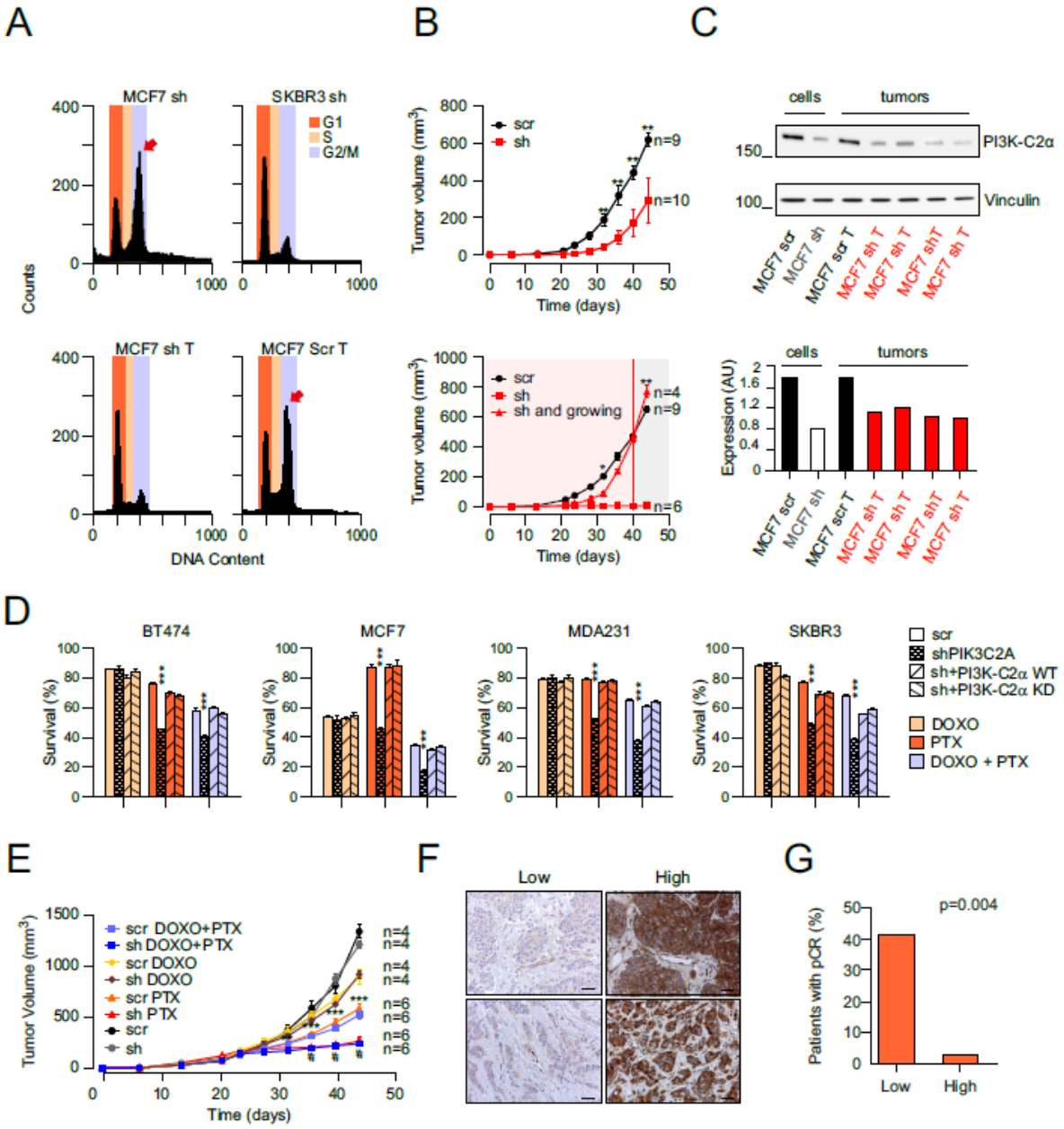
A
B
C
MCF7 sh
SKBR3 sh
G1
S
G2/M
Counts
MCF7 sh T
MCF7 Scr T
DNA Content
Tumor volume (mm3)
scr
sh
sh and growing
n=9
n=10
n=4
n=6
Time (days)
cells
tumors
PI3K-C2α
Vinculin
MCF7 scr
MCF7 sh
MCF7 scr T
MCF7 sh T
MCF7 shT
Expression (AU)
D
BT474
MCF7
MDA231
SKBR3
Survival (%)
scr
shPIK3C2A
sh+PI3K-C2α WT
sh+PI3K-C2α KD
DOXO
PTX
DOXO + PTX
E
Tumor Volume (mm3)
scr DOXO+PTX
sh DOXO+PTX
scr DOXO
sh DOXO
scr PTX
sh PTX
scr
sh
n=4
n=6
Time (days)
F
Low
High
G
p=0.004
Patients with pCR (%)

Figure 7. Role of PI3K-C2α in human breast cancer

A, PI staining and FACS analysis of shRNA-PI3K-C2α MCF7 (MCF7 sh), shRNA-PI3K-C2α SKBR3 (SKBR3 sh), shRNA-PI3K-C2α MCF7 derived from explanted tumors (MCF7 sh T) and Scramble MCF7 derived from explanted tumors (MCF7 Scr T) treated with 100 ng/ml Nocodazole for 16 hours. Red arrows G2/M peak. **B**, Tumor growth curve of scramble (Scr) and shRNA-PI3K-C2α MCF7 xenografts in NSG mice. Upper graph, tumor volume quantification of scramble (n=9) vs shRNA (n=10) MCF7. Bottom graph, tumor volume quantification of scramble (circles, n=9) and shRNA-treated MCF7cells (growth arrested, squares, n=6; or growing, triangles, n=4). The red shaded background indicates the early stage of tumors while the gray one the late phase. Results are shown as mean ± SEM. **C**, PI3K-C2α expression was assessed by WB analysis in indicated cell lines and primary tumors. WCL lysates were immunoblotted with indicated antibodies (n=3). **D**, Cell survival analyses of Scramble (Scr), shRNA-PI3K-C2α, sh+PI3K-C2α WT and sh+PI3K-C2α KD breast cancer cell lines (BT474, MCF7, MDA231 and SKBR3) after incubating with PTX, DOXO or a combination of the two drugs (PTX+DOXO) for 24 hr. Cell survival was determined by MTT assays as ratio of live cells after treatment compared with live cells treated with vehicle. Results are shown as mean ± SEM (n=3). **E**, Effect of PTX (n=6), DOXO (n=4) or combination of the two drugs (PTX+DOXO) (n=6) on tumor growth of scramble (Scr) and shRNA-PI3K-C2α (sh) SKBR3 xenografts in NSG mice (untreated mice n=4). Results are shown as mean ± SEM. **F**, Immunohistochemical (IHC) assessment of the level of PI3K-C2α expression. Left panel, cases with low staining are scored as IHC score 1. Right panel, cases showing positivity to PI3K-C2α staining (IHC score 3) (×40) (n=43 patients). Scale bars: 40 μm. **G**, PI3K-C2α and pathological complete response (pCR) after ATx6 chemotherapy regimen (n=43 patients).

Unless otherwise indicated, *p<0.05, **p<0.01; ***p<0.001; by analysis of variance (ANOVA) followed by Bonferroni post-hoc test.

References

Abraham, G., Kowalczyk, A., Loi, S., Haviv, I., and Zobel, J. (2010). Prediction of breast cancer prognosis using gene set statistics provides signature stability and biological context. BMC Bioinformatics *11*, 277.

Amaro, A. C., Samora, C. P., Holtackers, R., Wang, E., Kingston, I. J., Alonso, M., Lampson, M., McAinsh, A. D., and Meraldi, P. (2010). Molecular control of kinetochore-microtubule dynamics and chromosome oscillations. Nat Cell Biol *12*, 319-329.

Balmativola, D., Marchio, C., Maule, M., Chiusa, L., Annaratone, L., Maletta, F., Montemurro, F., Kulka, J., Figueiredo, P., Varga, Z., *et al.* (2014). Pathological non-response to chemotherapy in a neoadjuvant setting of breast cancer: an inter-institutional study. Breast Cancer Res Treat *148*, 511-523.

Bird, A. W., and Hyman, A. A. (2008). Building a spindle of the correct length in human cells requires the interaction between TPX2 and Aurora A. J Cell Biol *182*, 289-300.

Booth, D. G., Hood, F. E., Prior, I. A., and Royle, S. J. (2011). A TACC3/ch-TOG/clathrin complex stabilises kinetochore fibres by inter-microtubule bridging. EMBO J *30*, 906-919.

Campa, C. C., Martini, M., De Santis, M. C., and Hirsch, E. (2015). How PI3K-derived lipids control cell division. Front Cell Dev Biol *3*, 61.

Castedo, M., Perfettini, J. L., Roumier, T., Andreau, K., Medema, R., and Kroemer, G. (2004). Cell death by mitotic catastrophe: a molecular definition. Oncogene *23*, 2825-2837.

Cerami, E., Gao, J., Dogrusoz, U., Gross, B. E., Sumer, S. O., Aksoy, B. A., Jacobsen, A., Byrne, C. J., Heuer, M. L., Larsson, E., *et al.* (2012). The cBio cancer genomics portal: an open platform for exploring multidimensional cancer genomics data. Cancer Discov *2*, 401-404.

Cheeseman, L. P., Harry, E. F., McAinsh, A. D., Prior, I. A., and Royle, S. J. (2013). Specific removal of TACC3-ch-TOG-clathrin at metaphase deregulates kinetochore fiber tension. J Cell Sci *126*, 2102-2113.

Chen, J. G., and Horwitz, S. B. (2002). Differential mitotic responses to microtubule-stabilizing and -destabilizing drugs. Cancer Res *62*, 1935-1938.

Ciraolo, E., Gulluni, F., and Hirsch, E. (2014). Methods to measure the enzymatic activity of PI3Ks. Methods Enzymol *543*, 115-140.

Coates, A. S., Winer, E. P., Goldhirsch, A., Gelber, R. D., Gnant, M., Piccart-Gebhart, M., Thurlimann, B., and Senn, H. J. (2015). -Tailoring therapies-improving the management of early breast cancer: St Gallen International Expert Consensus on the Primary Therapy of Early Breast Cancer 2015. Ann Oncol *26*, 1533-1546.

Colombo, R., Caldarelli, M., Mennecozzi, M., Giorgini, M. L., Sola, F., Cappella, P., Perrera, C., Depaolini, S. R., Rusconi, L., Cucchi, U., *et al.* (2010). Targeting the mitotic checkpoint for cancer therapy with NMS-P715, an inhibitor of MPS1 kinase. Cancer Res *70*, 10255-10264.

De Antoni, A., Pearson, C. G., Cimini, D., Canman, J. C., Sala, V., Nezi, L., Mapelli, M., Sironi, L., Faretta, M., Salmon, E. D., and Musacchio, A. (2005). The Mad1/Mad2 complex as a template for Mad2 activation in the spindle assembly checkpoint. Curr Biol *15*, 214-225.

De Santis, M. C., Sala, V., Martini, M., Ferrero, G. B., and Hirsch, E. (2017). PI3K Signaling in Tissue Hyper-Proliferation: From Overgrowth Syndromes to Kidney Cysts. Cancers *9*.

Derry, W. B., Wilson, L., and Jordan, M. A. (1995). Substoichiometric binding of taxol suppresses microtubule dynamics. Biochemistry *34*, 2203-2211.

Domin, J., Gaidarov, I., Smith, M. E., Keen, J. H., and Waterfield, M. D. (2000). The class II phosphoinositide 3-kinase PI3K-C2alpha is concentrated in the trans-Golgi network and present in clathrin-coated vesicles. J Biol Chem *275*, 11943-11950.

Dubsky, P., Brase, J. C., Jakesz, R., Rudas, M., Singer, C. F., Greil, R., Dietze, O., Luisser, I., Klug, E., Sedivy, R., *et al.* (2013). The EndoPredict score provides prognostic information on late distant metastases in ER+/HER2- breast cancer patients. Br J Cancer *109*, 2959-2964.

Elis, W., Triantafellow, E., Wolters, N. M., Sian, K. R., Caponigro, G., Borawski, J., Gaither, L. A., Murphy, L. O., Finan, P. M., and Mackeigan, J. P. (2008). Down-regulation of class II phosphoinositide 3-kinase alpha expression below a critical threshold induces apoptotic cell death. Mol Cancer Res *6*, 614-623.

Franco, I., Gulluni, F., Campa, C. C., Costa, C., Margaria, J. P., Ciraolo, E., Martini, M., Monteyne, D., De Luca, E., Germena, G., *et al.* (2014). PI3K class II alpha controls spatially restricted endosomal PtdIns3P and Rab11 activation to promote primary cilium function. Dev Cell *28*, 647-658.

Franco, I., Margaria, J. P., De Santis, M. C., Ranghino, A., Monteyne, D., Chiaravalli, M., Pema, M., Campa, C. C., Ratto, E., Gulluni, F., *et al.* (2015). Phosphoinositide 3-Kinase-C2alpha Regulates Polycystin-2 Ciliary Entry and Protects against Kidney Cyst Formation. J Am Soc Nephrol.

Franco, S., Gostissa, M., Zha, S., Lombard, D. B., Murphy, M. M., Zarrin, A. A., Yan, C., Tepsuporn, S., Morales, J. C., Adams, M. M., *et al.* (2006). H2AX prevents DNA breaks from progressing to chromosome breaks and translocations. Mol Cell *21*, 201-214.

Fu, J., Bian, M., Xin, G., Deng, Z., Luo, J., Guo, X., Chen, H., Wang, Y., Jiang, Q., and Zhang, C. (2015). TPX2 phosphorylation maintains metaphase spindle length by regulating microtubule flux. J Cell Biol *210*, 373-383.

Gaidarov, I., Smith, M. E., Domin, J., and Keen, J. H. (2001). The class II phosphoinositide 3-kinase C2alpha is activated by clathrin and regulates clathrin-mediated membrane trafficking. Mol Cell *7*, 443-449.

Gaidarov, I., Zhao, Y., and Keen, J. H. (2005). Individual phosphoinositide 3-kinase C2alpha domain activities independently regulate clathrin function. J Biol Chem *280*, 40766-40772.

Gao, J., Aksoy, B. A., Dogrusoz, U., Dresdner, G., Gross, B., Sumer, S. O., Sun, Y., Jacobsen, A., Sinha, R., Larsson, E., *et al.* (2013). Integrative analysis of complex cancer genomics and clinical profiles using the cBioPortal. Sci Signal *6*, pl1.

Gascoigne, K. E., and Taylor, S. S. (2009). How do anti-mitotic drugs kill cancer cells? J Cell Sci *122*, 2579-2585.

Gasic, I., Nerurkar, P., and Meraldi, P. (2015). Centrosome age regulates kinetochore-microtubule stability and biases chromosome mis-segregation. Elife *4*.

Gassmann, R., Holland, A. J., Varma, D., Wan, X., Civril, F., Cleveland, D. W., Oegema, K., Salmon, E. D., and Desai, A. (2010). Removal of Spindly from microtubule-attached kinetochores controls spindle checkpoint silencing in human cells. Genes Dev *24*, 957-971.

Ghigo, A., Li, M., and Hirsch, E. (2016). New signal transduction paradigms in anthracycline-induced cardiotoxicity. Biochim Biophys Acta *1863*, 1916-1925.

Goldhirsch, A., Wood, W. C., Coates, A. S., Gelber, R. D., Thurlimann, B., and Senn, H. J. (2011). Strategies for subtypes--dealing with the diversity of breast cancer: highlights of the St. Gallen International Expert Consensus on the Primary Therapy of Early Breast Cancer 2011. Ann Oncol *22*, 1736-1747.

Goldhirsch, A., Wood, W. C., Gelber, R. D., Coates, A. S., Thurlimann, B., and Senn, H. J. (2007). Progress and promise: highlights of the international expert consensus on the primary therapy of early breast cancer 2007. Ann Oncol *18*, 1133-1144.

Gulluni, F., Martini, M., De Santis, M. C., Campa, C. C., Ghigo, A., Margaria, J. P., Ciraolo, E., Franco, I., Ala, U., Annaratone, L., *et al.* (2017). Mitotic Spindle Assembly and Genomic Stability in Breast Cancer Require PI3K-C2alpha Scaffolding Function. Cancer cell *32*, 444-459 e447.

Hanahan, D., and Weinberg, R. A. (2011). Hallmarks of cancer: the next generation. Cell *144*, 646-674.

Hatzis, C., Pusztai, L., Valero, V., Booser, D. J., Esserman, L., Lluch, A., Vidaurre, T., Holmes, F., Souchon, E., Wang, H., *et al.* (2011). A genomic predictor of response and survival following taxane-anthracycline chemotherapy for invasive breast cancer. JAMA *305*, 1873-1881.

Hood, F. E., Williams, S. J., Burgess, S. G., Richards, M. W., Roth, D., Straube, A., Pfuhl, M., Bayliss, R., and Royle, S. J. (2013). Coordination of adjacent domains mediates TACC3-ch-TOG-clathrin assembly and mitotic spindle binding. J Cell Biol *202*, 463-478.

Hubner, N. C., Bird, A. W., Cox, J., Splettstoesser, B., Bandilla, P., Poser, I., Hyman, A., and Mann, M. (2010). Quantitative proteomics combined with BAC TransgeneOmics reveals in vivo protein interactions. J Cell Biol *189*, 739-754.

Hudis, C. A., Barlow, W. E., Costantino, J. P., Gray, R. J., Pritchard, K. I., Chapman, J. A., Sparano, J. A., Hunsberger, S., Enos, R. A., Gelber, R. D., and Zujewski, J. A. (2007). Proposal for standardized definitions for efficacy end points in adjuvant breast cancer trials: the STEEP system. J Clin Oncol *25*, 2127-2132.

Jordan, M. A., Toso, R. J., Thrower, D., and Wilson, L. (1993). Mechanism of mitotic block and inhibition of cell proliferation by taxol at low concentrations. Proc Natl Acad Sci U S A *90*, 9552-9556.

Kim, S., Sun, H., Ball, H. L., Wassmann, K., Luo, X., and Yu, H. (2010). Phosphorylation of the spindle checkpoint protein Mad2 regulates its conformational transition. Proc Natl Acad Sci U S A *107*, 19772-19777.

Koch, A., Maia, A., Janssen, A., and Medema, R. H. (2016). Molecular basis underlying resistance to Mps1/TTK inhibitors. Oncogene *35*, 2518-2528.

Liu, S., Liu, W., Jakubczak, J. L., Erexson, G. L., Tindall, K. R., Chan, R., Muller, W. J., Adhya, S., Garges, S., and Merlino, G. (2002). Genetic instability favoring transversions associated with ErbB2-induced mammary tumorigenesis. Proc Natl Acad Sci U S A *99*, 3770-3775.

Luo, Y., Ran, J., Xie, S., Yang, Y., Chen, J., Li, S., Shui, W., Li, D., Liu, M., and Zhou, J. (2016). ASK1 controls spindle orientation and positioning by phosphorylating EB1 and stabilizing astral microtubules. Cell Discov *2*, 16033.

Martin, M., Romero, A., Cheang, M. C., Lopez Garcia-Asenjo, J. A., Garcia-Saenz, J. A., Oliva, B., Roman, J. M., He, X., Casado, A., de la Torre, J., *et al.* (2011). Genomic predictors of response to doxorubicin versus docetaxel in primary breast cancer. Breast Cancer Res Treat *128*, 127-136.

Martini, M., De Santis, M. C., Braccini, L., Gulluni, F., and Hirsch, E. (2014). PI3K/AKT signaling pathway and cancer: an updated review. Annals of medicine *46*, 372-383.

Meraldi, P., Draviam, V. M., and Sorger, P. K. (2004). Timing and checkpoints in the regulation of mitotic progression. Dev Cell *7*, 45-60.

Pinder, S. E., and Reis-Filho, J. S. (2007). Non-operative breast pathology. J Clin Pathol *60*, 1297-1299.

Posor, Y., Eichhorn-Gruenig, M., Puchkov, D., Schoneberg, J., Ullrich, A., Lampe, A., Muller, R., Zarbakhsh, S., Gulluni, F., Hirsch, E., *et al.* (2013). Spatiotemporal control of endocytosis by phosphatidylinositol-3,4-bisphosphate. Nature *499*, 233-+.

Prowell, T. M., and Pazdur, R. (2012). Pathological complete response and accelerated drug approval in early breast cancer. The New England journal of medicine *366*, 2438-2441.

Qi, W., and Yu, H. (2007). KEN-box-dependent degradation of the Bub1 spindle checkpoint kinase by the anaphase-promoting complex/cyclosome. J Biol Chem *282*, 3672-3679.

Quaglino, E., Iezzi, M., Mastini, C., Amici, A., Pericle, F., Di Carlo, E., Pupa, S. M., De Giovanni, C., Spadaro, M., Curcio, C., *et al.* (2004). Electroporated DNA vaccine clears away multifocal mammary carcinomas in her-2/neu transgenic mice. Cancer Res *64*, 2858-2864.

Ricke, R. M., Jeganathan, K. B., and van Deursen, J. M. (2011). Bub1 overexpression induces aneuploidy and tumor formation through Aurora B kinase hyperactivation. J Cell Biol *193*, 1049-1064.

Rieder, C. L., and Maiato, H. (2004). Stuck in division or passing through: what happens when cells cannot satisfy the spindle assembly checkpoint. Dev Cell *7*, 637-651.

Royle, S. J. (2013). Protein adaptation: mitotic functions for membrane trafficking proteins. Nat Rev Mol Cell Biol *14*, 592-599.

Salmon, E. D., and Begg, D. A. (1980). Functional implications of cold-stable microtubules in kinetochore fibers of insect spermatocytes during anaphase. J Cell Biol *85*, 853-865.

Santaguida, S., Tighe, A., D'Alise, A. M., Taylor, S. S., and Musacchio, A. (2010). Dissecting the role of MPS1 in chromosome biorientation and the spindle checkpoint through the small molecule inhibitor reversine. J Cell Biol *190*, 73-87.

Santaguida, S., Vernieri, C., Villa, F., Ciliberto, A., and Musacchio, A. (2011). Evidence that Aurora B is implicated in spindle checkpoint signalling independently of error correction. EMBO J *30*, 1508-1519.

Schmidt, S., Schneider, L., Essmann, F., Cirstea, I. C., Kuck, F., Kletke, A., Janicke, R. U., Wiek, C., Hanenberg, H., Ahmadian, M. R., *et al.* (2010). The centrosomal protein TACC3 controls paclitaxel sensitivity by modulating a premature senescence program. Oncogene *29*, 6184-6192.

Serio, G., Margaria, V., Jensen, S., Oldani, A., Bartek, J., Bussolino, F., and Lanzetti, L. (2011). Small GTPase Rab5 participates in chromosome congression and regulates localization of the centromere-associated protein CENP-F to kinetochores. Proc Natl Acad Sci U S A *108*, 17337-17342.

Sorrentino, V., Nelson, J. K., Maspero, E., Marques, A. R., Scheer, L., Polo, S., and Zelcer, N. (2013). The LXR-IDOL axis defines a clathrin-, caveolae-, and dynamin-independent endocytic route for LDLR internalization and lysosomal degradation. J Lipid Res *54*, 2174-2184.

Traer, C. J., Foster, F. M., Abraham, S. M., and Fry, M. J. (2006). Are class II phosphoinositide 3-kinases potential targets for anticancer therapies? Bull Cancer *93*, E53-58.

van 't Veer, L. J., Dai, H., van de Vijver, M. J., He, Y. D., Hart, A. A., Mao, M., Peterse, H. L., van der Kooy, K., Marton, M. J., Witteveen, A. T., *et al.* (2002). Gene expression profiling predicts clinical outcome of breast cancer. Nature *415*, 530-536.

Vanhaesebroeck, B., Guillermet-Guibert, J., Graupera, M., and Bilanges, B. (2010). The emerging mechanisms of isoform-specific PI3K signalling. Nat Rev Mol Cell Biol *11*, 329-341.

Vitre, B., Gudimchuk, N., Borda, R., Kim, Y., Heuser, J. E., Cleveland, D. W., and Grishchuk, E. L. (2014). Kinetochore-microtubule attachment throughout mitosis potentiated by the elongated stalk of the kinetochore kinesin CENP-E. Mol Biol Cell *25*, 2272-2281.

Weaver, B. A. (2014). How Taxol/paclitaxel kills cancer cells. Mol Biol Cell *25*, 2677-2681.

Yoshioka, K., Yoshida, K., Cui, H., Wakayama, T., Takuwa, N., Okamoto, Y., Du, W., Qi, X., Asanuma, K., Sugihara, K., *et al.* (2012). Endothelial PI3K-C2alpha, a class II PI3K, has an essential role in angiogenesis and vascular barrier function. Nat Med *18*, 1560-1569.

Supplementary Figures

Figure S1

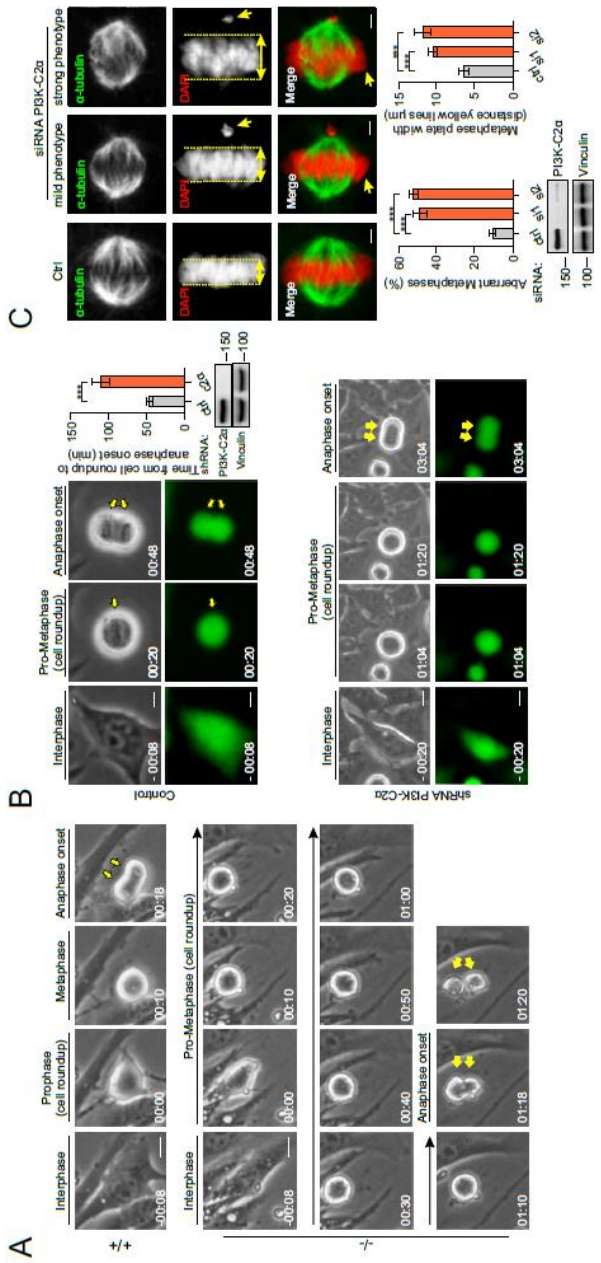

Figure S1, related to Figure 1

(A) Representative pictures of time lapse analysis from cell round up to anaphase onset (chromosome segregation/cellular elongation indicated by yellow arrows) of WT and *Pik3c2a*$^{-/-}$ MEFs (n= 100 cells). (**B**) Representative pictures of time lapse analysis from cell roundup to anaphase onset (chromosome segregation/cellular elongation indicated by yellow arrows) of HeLa subjected to scramble TurboGFP control, TurboGFP-shRNA-mediated silencing against PI3K-C2α and relative quantification (n=100). Results are shown as mean ± SEM. Western blot validation of PI3K-C2α downregulation. Whole-cell lysates (WCL) were immunoblotted with indicated antibodies. (**C)** Immunofluorescence staining of metaphase spindle length and chromosome plate width and relative quantifications of siRNA-treated HeLa cells (control cells were transfected with scramble siRNA) (n=100). Results are shown as mean ± SEM (n=100). Western blot validation of PI3K-C2α downregulation. WCL lysates were immunoblotted with indicated antibodies

Unless otherwise indicated, ***$p<0.001$; by analysis of variance (ANOVA). Data are representative of at least three independent experiments.

Figure S2

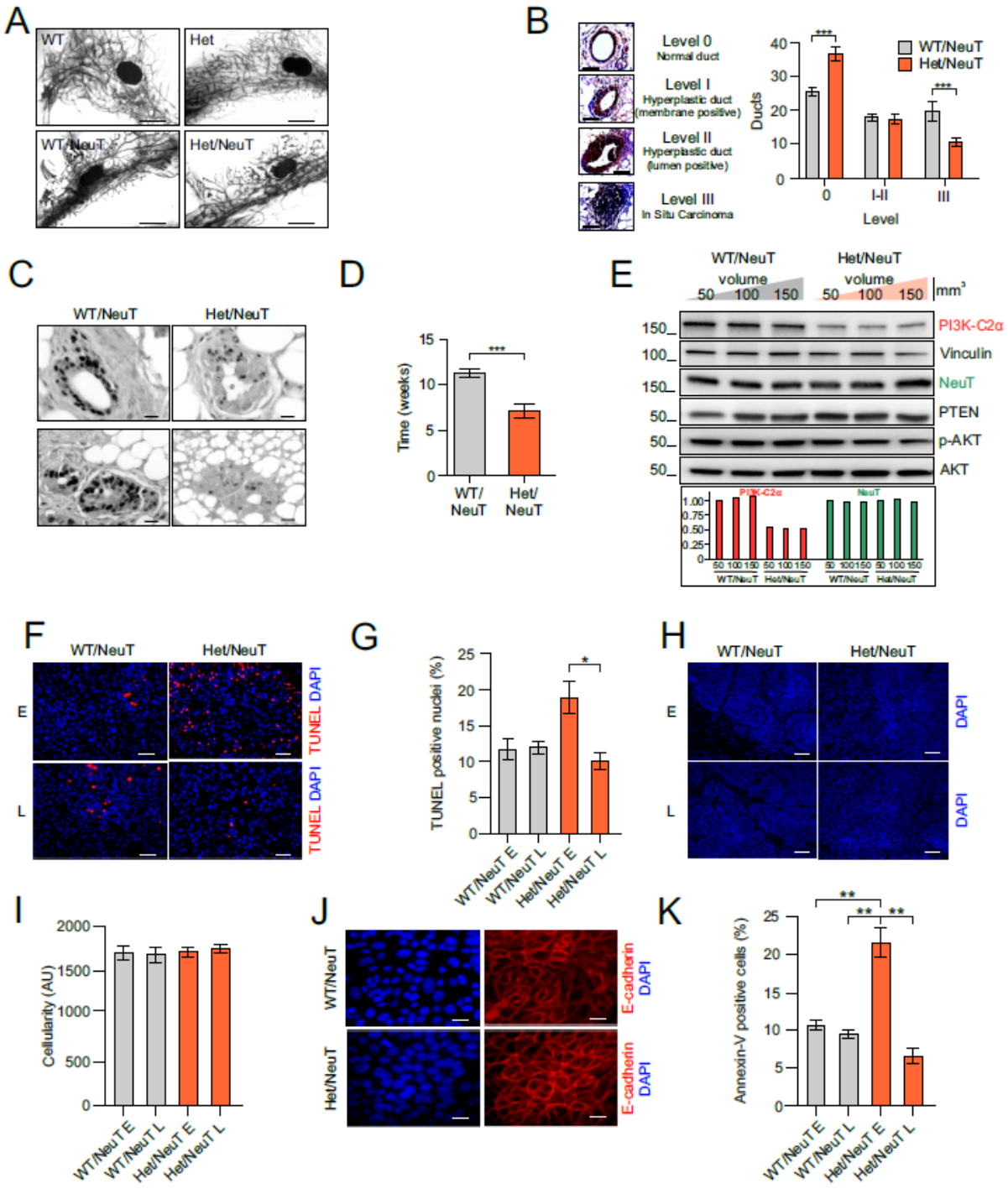
A
WT
Het
WT/NeuT
Het/NeuT
B
Level 0
Normal duct
Level I
Hyperplastic duct
(membrane positive)
Level II
Hyperplastic duct
(lumen positive)
Level III
In Situ Carcinoma
Ducts
WT/NeuT
Het/NeuT
0
I-II
III
Level
C
WT/NeuT
Het/NeuT
D
Time (weeks)
WT/ NeuT
Het/ NeuT
E
WT/NeuT
Het/NeuT
volume
50 100 150
mm³
PI3K-C2α
Vinculin
NeuT
PTEN
p-AKT
AKT
F
WT/NeuT
Het/NeuT
E
L
TUNEL DAPI
G
TUNEL positive nuclei (%)
WT/NeuT E
WT/NeuT L
Het/NeuT E
Het/NeuT L
H
WT/NeuT
Het/NeuT
E
L
DAPI
I
Cellularity (AU)
J
WT/NeuT
Het/NeuT
E-cadherin
DAPI
K
Annexin-V positive cells (%)

Figure S2, related to Figure 2

(A) Histological sections of the fourth pair of virgin mammary glands. Glands pictured illustrate morphology representative of each genotype at 6/8 weeks of age (n=6 mice). Scale bar: 2 mm. (**B)** *NeuT/Pik3c2a*$^{+/+}$ (Wt/NeuT) and *NeuT/Pik3c2a*$^{+/-}$ (Het/NeuT) lesions in the fourth pair of mammary glands. The lesions were graded using the criteria outlined in the STAR Methods section to approximate the scoring system in place for human surgical specimen: level 0, normal ducts; level 1, mild hyperplasia with multiple layers; level 2, moderate hyperplasia and atypical hyperplasia; level 3, in situ carcinoma. Results are shown as mean ± SEM (n=6 mice, 100 ducts scored for each mouse). Scale bar: 60 μm. (**C)** Immunohistochemical expression of Proliferating Nuclear Cellular Antigen (PCNA) in mammary glands (fourth pair) at 8 weeks of age (n=6 mice). (**D)** Speed of growth of NeuT tumors in the fourth pair of mammary glands. Speed of growth was calculated as the time taken by a tumor to grow from 1 mm to 4 mm in diameter. Results are shown as mean ± SEM (n=20 mice for Wt/NeuT and n=25 mice for Het/NeuT). Scale bar: 20 μm. (**E)** Western blot analysis of Wt/NeuT and Het/NeuT primary tumors of increasing volumes and relative quantification. WCL were immunoblotted with indicated antibodies (n=3). (**F-G**) TUNEL and DAPI staining (**F**) of NeuT tumors (fourth pair of mammary glands) at early (E) and late (L) stage and relative quantification (**G**). Results are shown as mean ± SEM (n=4). Scale bar: 50 μm. (**H-I**) DAPI staining (**H**) of NeuT tumors (fourth pair of mammary glands) at early (E) and late (L) stage and relative quantification (**I**). Results are shown as mean ± SEM (n=4). Scale bar: 80 μm. (**J**) Immunofluorescence expression of E-Cadherin marker in MMET (Murine Mammalian Epithelial Tumors) cell lines (n=3). Scale bar: 20 μm. (**K**) FACS analysis of E and L Wt/NeuT and Het/NeuT MMET cells to score apoptosis (Annexin V staining). Results are shown as mean ± SEM (n=4).
Unless otherwise indicated, *$p<0.05$, **$p<0.01$; ***$p<0.001$; by analysis of variance (ANOVA). Data are representative of at least three independent experiments.

Figure S3

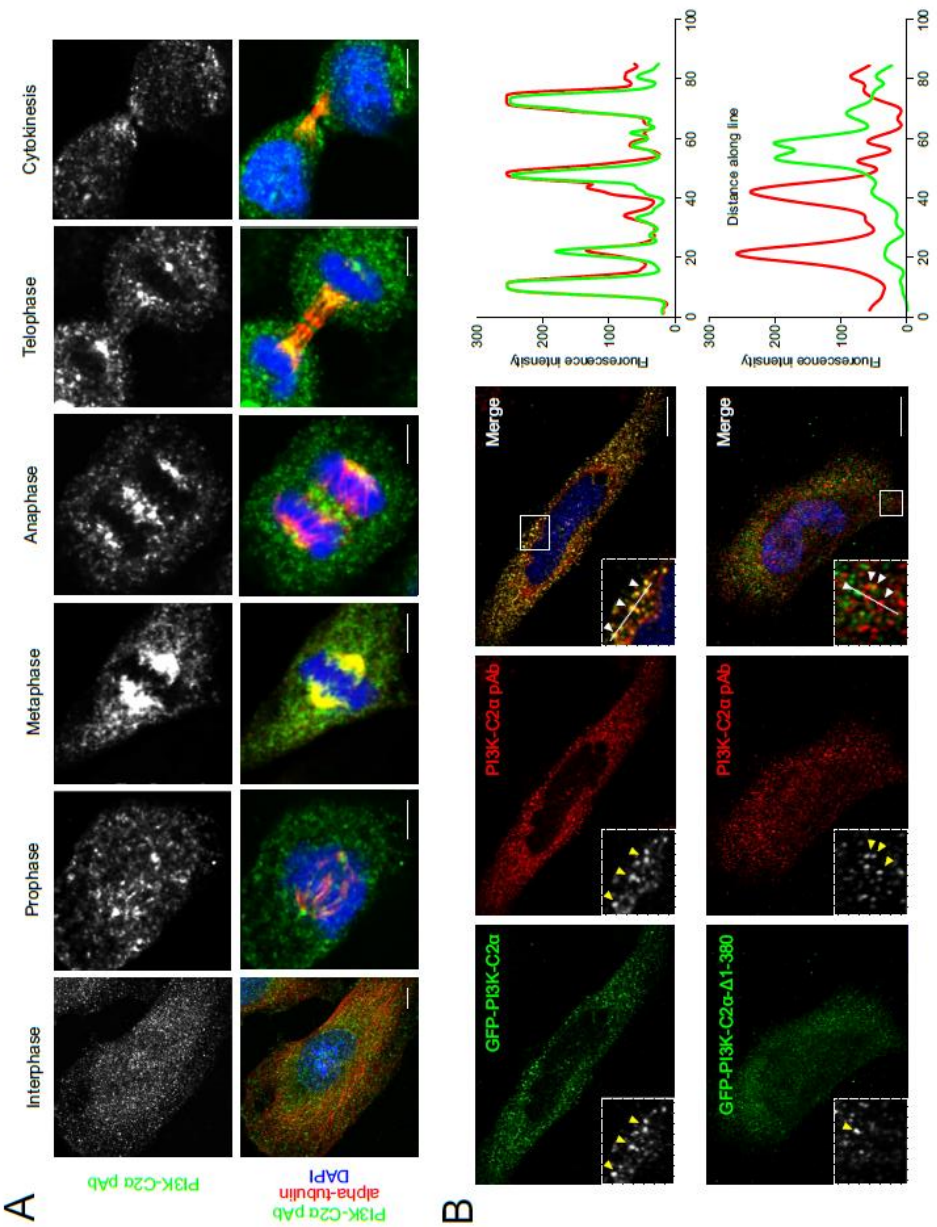
A
Interphase
Prophase
Metaphase
Anaphase
Telophase
Cytokinesis
PI3K-C2α pAb
PI3K-C2α pAb
alpha-tubulin
DAPI
B
GFP-PI3K-C2α
PI3K-C2α pAb
Merge
GFP-PI3K-C2α-Δ1-380
PI3K-C2α pAb
Merge
Fluorescence intensity
Distance along line
Fluorescence intensity

Figure S3, related to Figure 3

(A) Immunofluorescence staining of anti-PI3K-C2α (green), anti-alpha tubulin (red) and DAPI in all the phases of mitosis. (n=3). **(B**) Immunofluorescence staining of anti-PI3K-C2α antibody (red) and GFP-PI3K-C2α WT and Δ1-380 (green). Upper panels showed co-localization between the antibody and WT PI3K-C2α confirming the specificity of the antibody. Anti-PI3K-C2α antibody was raised on N-terminal region (1-338aa) and as expected no co-localization to GFP-PI3K-C2α Δ1-380 was observed in lower panels. (n=3)

Data are representative of at least three independent experiments.

Figure S4

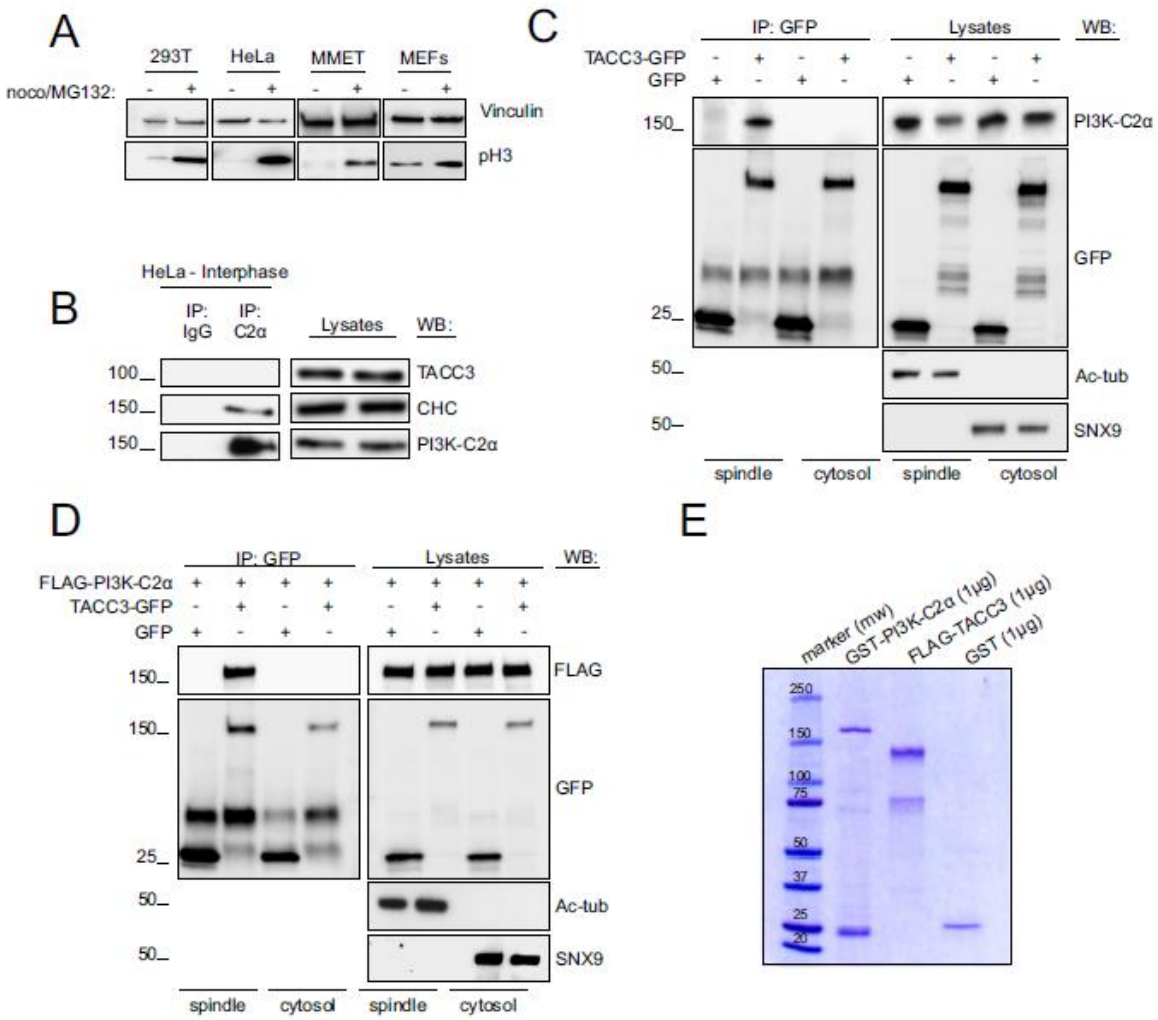
A
293T
HeLa
MMET
MEFs
noco/MG132:
Vinculin
pH3
B
HeLa - Interphase
IP: IgG
IP: C2α
Lysates
WB:
100_
150_
150_
TACC3
CHC
PI3K-C2α
C
IP: GFP
Lysates
WB:
TACC3-GFP
GFP
150_
25_
50_
50_
PI3K-C2α
GFP
Ac-tub
SNX9
spindle
cytosol
spindle
cytosol
D
IP: GFP
Lysates
WB:
FLAG-PI3K-C2α
TACC3-GFP
GFP
150_
150_
25_
50_
50_
FLAG
GFP
Ac-tub
SNX9
spindle
cytosol
spindle
cytosol
E
marker (mw)
GST-PI3K-C2α (1μg)
FLAG-TACC3 (1μg)
GST (1μg)
250
150
100
75
50
37
25
20

Figure S4, related to Figure 3

(A) Western blot analysis of HEK293T, HeLa, MMET and MEF untreated or treated with nocodazole (16h) followed by 2 hours release in fresh medium in the presence of 20μM MG132. WCL were immunoblotted with indicated antibodies (n=3). (**B**) PI3K-C2α was immunoprecipitated from the cell lysate of interphase-arrested HeLa cells with anti-PI3K-C2α antibody (IP) or control IgG. Bound proteins were detected by immunoblotting with anti-TACC3, anti-clathrin heavy chain (CHC) or anti-PI3K-C2α antibody (n=3). (**C)** HEK293T cells were transfected with GFP vector or GFP-TACC3. GFP-TACC3 was immunoprecipitated from cytoplasmic or spindle fraction of metaphase-arrested HEK293T cells with anti-GFP antibody (IP). Bound proteins were detected by immunoblotting with anti-PI3K-C2α and anti-GFP antibody (WB). Spindle fractionation quality was assessed using anti-acetylated tubulin (spindle fraction) and anti-SNX9 (cytosol fraction) antibody (WB) (n=5). (**D**) HEK293T cells were transfected with GFP vector or GFP-TACC3 and FLAG-PI3K-C2α. GFP-TACC3 was immunoprecipitated from cytoplasmic or spindle fraction of metaphase arrested HEK293T cells with anti-GFP antibody (IP). Bound proteins were detected by immunoblotting with anti-FLAG and anti-GFP antibody (WB). Spindle fractionation quality was assessed using anti-acetylated tubulin (spindle fraction) and anti-SNX9 (cytosol fraction) antibody (WB) (n=5). (**E**) Coomassie Brilliant Blue staining of the GST- PI3K-C2α, FLAG-TACC3 and GST recombinant proteins.

Data are representative of at least three independent experiments.

Figure S5

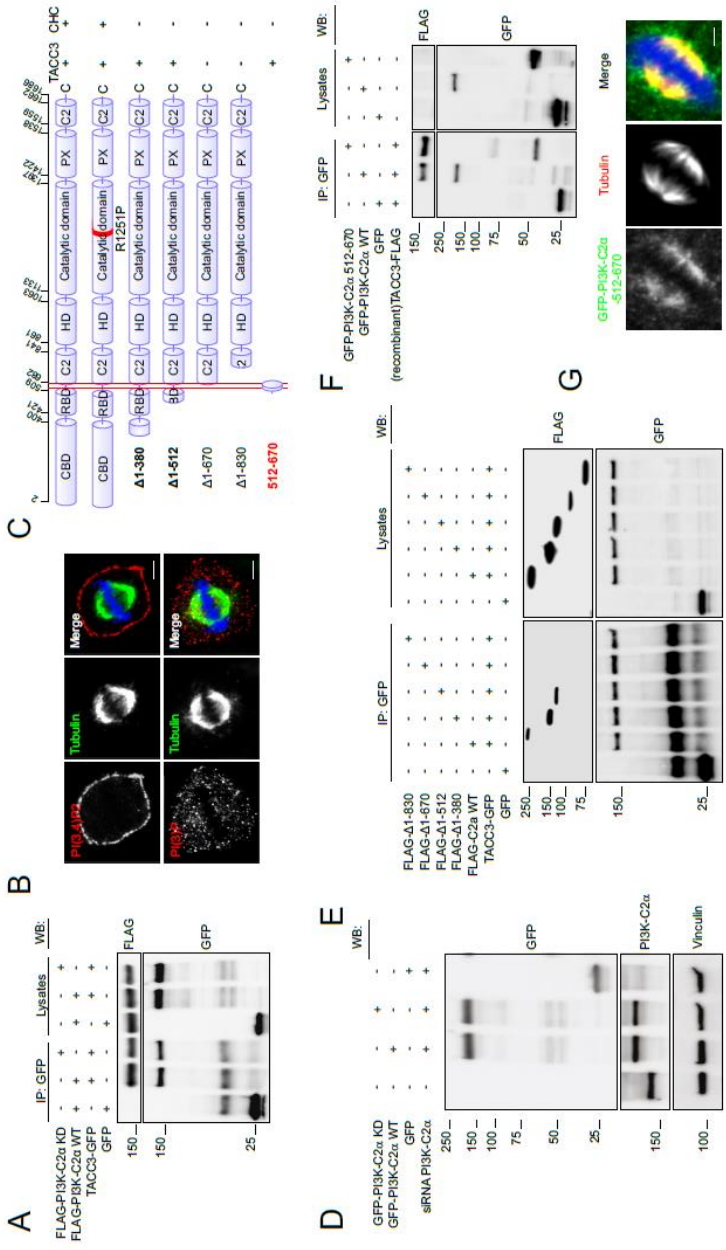
A
IP: GFP
Lysates
WB:
FLAG-PI3K-C2α KD
FLAG-PI3K-C2α WT
TACC3-GFP
GFP
FLAG
GFP
B
PI(3,4)P2
PI(3)P
Tubulin
Merge
C
CBD
RBD
C2
HD
Catalytic domain
PX
C2
C
TACC3
CHC
R1251P
Δ1-380
Δ1-512
Δ1-670
Δ1-830
512-670
D
GFP-PI3K-C2α KD
GFP-PI3K-C2α WT
GFP
siRNA PI3K-C2α
GFP
PI3K-C2α
Vinculin
E
FLAG-Δ1-830
FLAG-Δ1-670
FLAG-Δ1-512
FLAG-Δ1-380
FLAG-C2a WT
TACC3-GFP
GFP
FLAG
GFP
F
GFP-PI3K-C2α 512-670
GFP-PI3K-C2α WT
GFP
(recombinant)TACC3-FLAG
FLAG
GFP
G
GFP-PI3K-C2α 512-670
Tubulin
Merge

Figure S5, related to Figure 3

(A) HEK293T cells were transfected with GFP vector or FLAG-PI3K-C2α KD, FLAG-PI3K-C2α WT or GFP-TACC3. GFP-TACC3 was immunoprecipitated from metaphase-arrested HEK293T cells with anti-GFP antibody (IP). Bound proteins were detected by immunoblotting with anti-FLAG and anti-GFP antibody (WB). (**B)** Immunofluorescence staining of PI(3,4)P2 and PI(3)P in metaphase arrested HeLa cells (n=3). (**C)** Schematic representation of PI3K-C2α point and deletion mutants. (**D)** HeLa cells were transfected with GFP vector, GFP-PI3K-C2α KD or GFP-PI3K-C2α KD. WCL were immunoblotted with GPF, PI3K-C2α or vinculin antibody (n=3). (**E)** HEK293T cells were transfected with FLAG vector or FLAG-PI3K-C2α (wild-type or indicated deletion mutants). FLAG-PI3K-C2α (wild-type or deletion mutants) was immunoprecipitated in cell lysates of metaphase-arrested HEK293T cells with anti-FLAG antibody (IP). Bound proteins were blotted with anti-FLAG or anti-GFP antibody (WB) (n=6). (**F)** HEK293T cells were transfected with GFP vector, GFP-PI3K-C2α 512-670 or GFP-PI3K-C2α WT. GFP-PI3K-C2α 512-670 or GFP-PI3K-C2α WT was immunoprecipitated in cell lysates of metaphase-arrested HEK293T cells with anti-GFP antibody (IP) and incubated with recombinant FLAG-TACC3. Bound proteins were blotted with anti-FLAG or anti-GFP antibody (WB) (n=3). (**G)** Immunofluorescence staining of metaphase-arrested HeLa cells transfected with GFP-PI3K-C2α 512-670 (n=3).

Data are representative of at least three independent experiments.

Figure S6

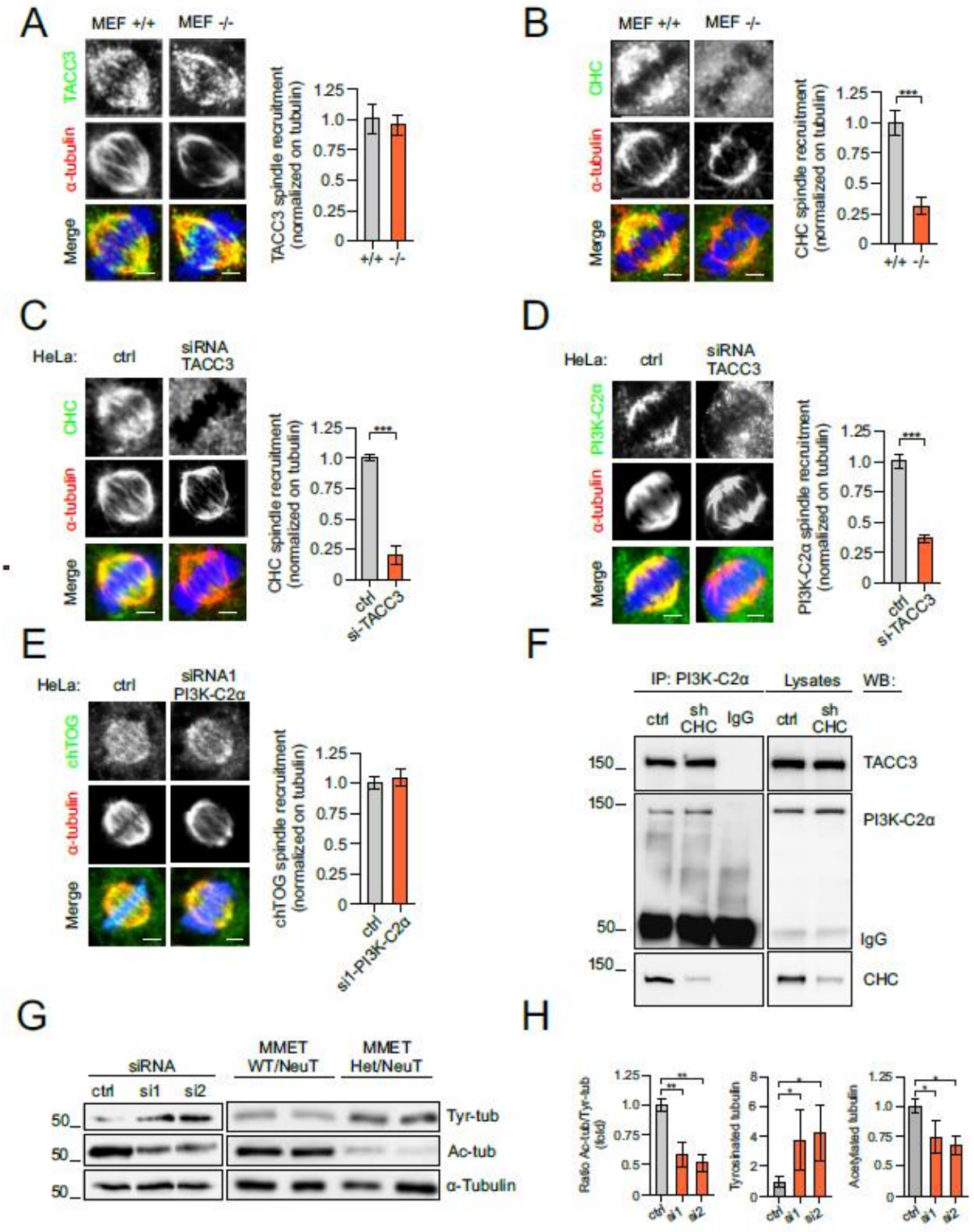
A
MEF +/+
MEF -/-
TACC3
α-tubulin
Merge
TACC3 spindle recruitment (normalized on tubulin)
+/+ -/-
B
CHC spindle recruitment (normalized on tubulin)
C
HeLa:
ctrl
siRNA TACC3
CHC spindle recruitment (normalized on tubulin)
ctrl
si-TACC3
D
PI3K-C2α
PI3K-C2α spindle recruitment (normalized on tubulin)
E
siRNA1 PI3K-C2α
chTOG
chTOG spindle recruitment (normalized on tubulin)
si1-PI3K-C2α
F
IP: PI3K-C2α
Lysates
WB:
sh CHC
IgG
TACC3
PI3K-C2α
CHC
G
siRNA
si1
si2
MMET WT/NeuT
MMET Het/NeuT
Tyr-tub
Ac-tub
α-Tubulin
H
Ratio Ac-tub/Tyr-tub (fold)
Tyrosinated tubulin
Acetylated tubulin

Figure S6, related to Figure 4

(A) Immunofluorescence staining and relative quantification of TACC3 recruitment on metaphase spindle in WT and *Pik3c2a*$^{-/-}$ MEFs. Results are shown as mean ± SEM (n=100). **(B)** Immunofluorescence staining and relative quantification of CHC recruitment on metaphase spindle in WT and *Pik3c2a*$^{-/-}$ MEFs. Results are shown as mean ± SEM (n=100). **(C)** Immunofluorescence staining and relative quantification of CHC recruitment on metaphase spindle in ctrl and TACC3 siRNA-treated HeLa cells. Results are shown as mean ± SEM (n=100). (**D)** Immunofluorescence staining and relative quantification of PI3K-C2α recruitment on metaphase spindle in ctrl and TACC3 siRNA-treated HeLa cells. Results are shown as mean ± SEM (n=100). (**E)** Immunofluorescence staining and relative quantification of chTOG recruitment on metaphase spindle in ctrl and PI3K-C2α siRNA-treated HeLa cells. Results are shown as mean ± SEM (n=100). (**F)** Inducible CHC knockdown HeLa cells were cultured in the presence of doxycycline for 6 days to induce silencing of the CHC. PI3K-C2α was immunoprecipitated in cell lysates of metaphase-arrested HeLa cells with anti- PI3K-C2α antibody (IP) or control IgG. Bound proteins were blotted with indicated antibodies (WB) (n=3). **(G)** Western blot analysis of acetylated/tyrosinated tubulin in the spindle fraction of PI3K-C2α siRNA-treated HeLa cells or MMET cells (n=3). **(H)** Quantification of acetylated and tyrosinated tubulin in PI3K-C2α siRNA-treated HeLa cells or MMET cells. Results are shown as mean ± SEM (n=100).

Unless otherwise indicated, *p<0.05, **p<0.01; ***p<0.001; by analysis of variance (ANOVA). Data are representative of at least three independent experiments.

Figure S7

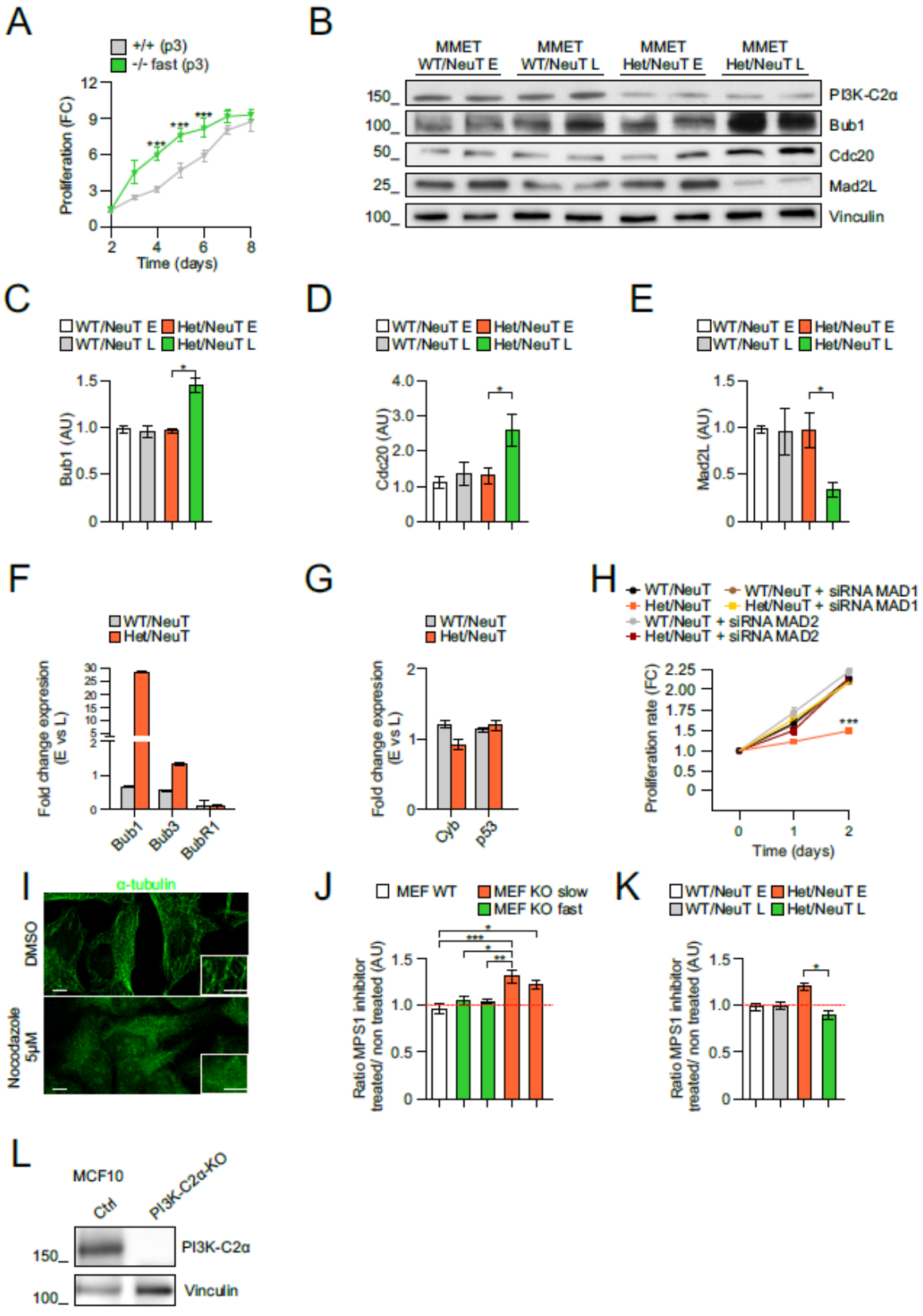
A
+/+ (p3)
-/- fast (p3)
Proliferation (FC)
Time (days)
B
MMET WT/NeuT E
MMET WT/NeuT L
MMET Het/NeuT E
MMET Het/NeuT L
PI3K-C2α
Bub1
Cdc20
Mad2L
Vinculin
C
WT/NeuT E
Het/NeuT E
WT/NeuT L
Het/NeuT L
Bub1 (AU)
D
Cdc20 (AU)
E
Mad2L (AU)
F
WT/NeuT
Het/NeuT
Fold change expresion (E vs L)
Bub1
Bub3
BubR1
G
Cyb
p53
H
WT/NeuT
Het/NeuT
WT/NeuT + siRNA MAD1
Het/NeuT + siRNA MAD1
WT/NeuT + siRNA MAD2
Het/NeuT + siRNA MAD2
Proliferation rate (FC)
Time (days)
I
α-tubulin
DMSO
Nocodazole 5μM
J
MEF WT
MEF KO slow
MEF KO fast
Ratio MPS1 inhibitor treated/ non treated (AU)
K
L
MCF10
Ctrl
PI3K-C2α-KO
PI3K-C2α
Vinculin

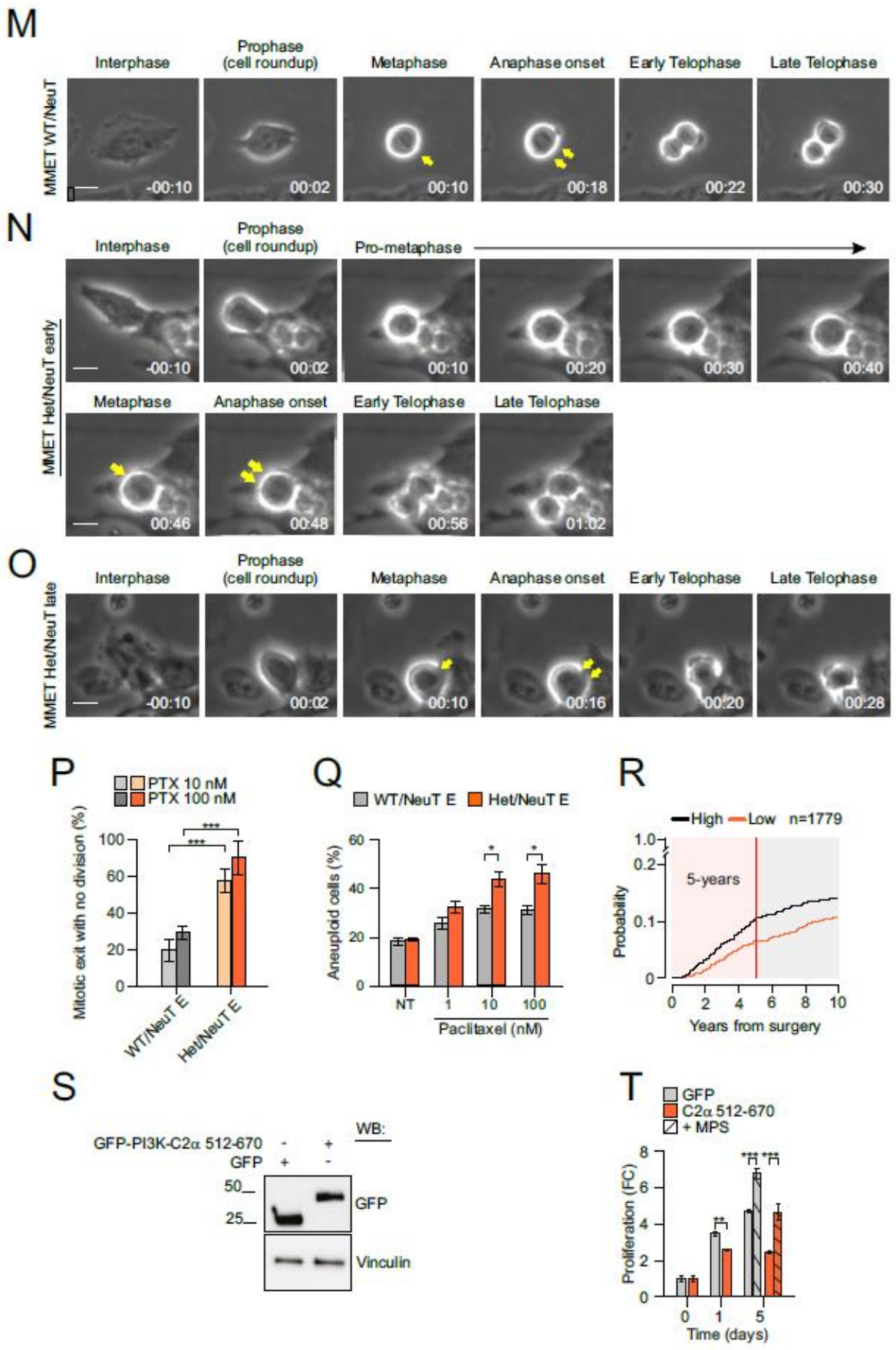
M
Interphase
Prophase (cell roundup)
Metaphase
Anaphase onset
Early Telophase
Late Telophase
MMET WT/NeuT
-00:10
00:02
00:10
00:18
00:22
00:30
N
Interphase
Prophase (cell roundup)
Pro-metaphase
MMET Het/NeuT early
-00:10
00:02
00:10
00:20
00:30
00:40
Metaphase
Anaphase onset
Early Telophase
Late Telophase
00:46
00:48
00:56
01:02
O
Interphase
Prophase (cell roundup)
Metaphase
Anaphase onset
Early Telophase
Late Telophase
MMET Het/NeuT late
-00:10
00:02
00:10
00:16
00:20
00:28
P
PTX 10 nM
PTX 100 nM
Mitotic exit with no division (%)
WT/NeuT E
Het/NeuT E
Q
WT/NeuT E
Het/NeuT E
Aneuploid cells (%)
NT
1
10
100
Paclitaxel (nM)
R
High
Low
n=1779
5-years
Probability
Years from surgery
S
GFP-PI3K-C2α 512-670
GFP
WB:
50
25
GFP
Vinculin
T
GFP
C2α 512-670
+ MPS
Proliferation (FC)
Time (days)

Figure S7, related to Figure 6

(A) Proliferation curve of WT MEFs and fast growing adapted populations of *Pik3c2a*$^{-/-}$ MEFs. FC, fold change. Results are shown as mean ± SEM (n=3) of populations stabilized for 3 passages (p3). **(B-E)** Western blot analysis (**B**) of Bub1, Cdc20 and Mad2L expression in MMET cells and relative quantification (**C-E**). Results are shown as mean ± SEM (n=5). (**F)** Quantitative Real Time PCR analysis of deregulated expression of Bub gene family in MMET cells. Results are shown as mean ± SEM (n=5). **(G)** Quantitative Real Time PCR analysis of deregulated expression of cyclin B1 and p53 genes in MMET cells. Results are shown as mean ± SEM (n=5). **(H)** Proliferation curve of control, MAD1 or MAD2 siRNA-treated WT/NeuT or Het/NeuT MMET cells. FC, fold change. Results are shown as mean ± SEM (n=8). **(I),** Immunofluorescence staining of α-tubulin in MMET cells treated with DMSO or 5μM Nocodazole. **(J-K)** Effect of spindle assembly checkpoint kinase MPS1 (MPSi) inhibitor on proliferation rate of WT and *Pik3c2a*$^{-/-}$ MEFs (**J**) and MMET (**K**). Results are shown as mean ± SD (n=5). **(L)** Western blot analysis of PI3K-C2α after CRISPR/Cas9 targeted deletion of *PIK3C2A* in MCF10A (n=3).

(M-O) Representative pictures of time lapse analysis from cell roundup to anaphase onset (chromosome segregation/cellular elongation indicated by yellow arrows) of Wt/NeuT (**M**), early Het/NeuT (**N**) and late Het/NeuT MMET (**O**) (n= 100 cells). **(P)** Time lapse analysis of early Wt/NeuT and Het/NeuT treated with 10 nM or 100 nM of Paclitaxel (PTX) or vehicle only. Percentage of cells exiting mitosis with no division was reported in graph. Results are shown as mean ± SD (n=100). **(Q)** FACS analysis of early Wt/NeuT and Het/NeuT MMET to score DNA content (PI staining) after treatment with Paclitaxel (indicated dosage, 24h). Results are shown as mean ± SEM (n=5). **(R)** Probability of distant event in breast cancer patients within 10 years showing that patients with low expression of PI3K-C2α (Low) are initially protected from tumor evolution (gray shading). The red shaded background the chart represents late events (after 5 years). (n= 1179 patients). **(S)** MCF7 cells were transfected with GFP vector or GFP-PI3K-C2α 512-670. WCL were blotted with anti-GFP antibody or Vinculin (WB) (representative blot of 3 independent experiments). **(T)** Effect of spindle assembly checkpoint kinase MPS1 (MPSi) inhibitor on proliferation rate of MCF7 cells transfected with GFP vector or GFP-PI3K-C2α 512-670. Results are shown as mean ± SEM of fold change (FC) (n=5).

Unless otherwise indicated, scale bars: 5 μm, *p<0.05, **p<0.01; ***p<0.001; by analysis of variance (ANOVA). Data are representative of at least three independent experiments.

Supplementary Tables

Table S1

Categories (n of chr)	MEF WT (%)	MEF KO (%)
50	0	2 (2.9)
60	0	3 (4.4)
61	0	1 (1.5)
62	0	2 (2.9)
63	0	3 (4.4)
64	0	3 (4.4)
65	0	9 (13.2)
66	0	2 (2.9)
67	0	4 (5.9)
68	0	8 (11.8)
69	0	3 (4.4)
70	0	6 (8.8)
71	0	0
72	0	0
73	0	4 (5.9)
74	0	7 (10.3)
75	0	3 (4.4)
76	0	3 (4.4)
77	0	4 (5.9)
78	0	0
79	0	1 (1.5)

Distribution of chromosome number in WT and *Pik3c2a* $^{-/-}$ MEFs.

Table S2

Sample	Total MP	Chromosome Breaks	Chromatid Breaks
+/+	22	1 (4.5%)	0 (0%)
-/-	31	10 (32%)	6 (19%)

Frequency of chromatid and chromosome breaks events

Table S3

Categories (n of chr)	MMET WT EARLY (%)	MMET WT LATE (%)	MMET HET EARLY (%)	MMET HET LATE (%)
50	4 (8.3)	0	0	0
60	1 (2.1)	0	0	1 (1.8)
61	0	2 (5.1)	0	0
62	1 (2.1)	0	0	1 (1.8)
63	1 (2.1)	1 (2.6)	1 (2.9)	0
64	0	0	0	1 (1.8)
65	0	0	1 (2.9)	0
66	0	1 (2.6)	0	1 (1.8)
67	0	0	0	0
68	0	1 (2.6)	0	1 (1.8)
69	0	0	0	1 (1.8)
70	0	1 (2.6)	1 (2.9)	1 (1.8)
71	0	1 (2.6)	0	0
72	0	0	0	1 (1.8)
73	0	0	1 (2.9)	0
74	0	1 (2.6)	0	2 (3.6)
75	0	0	0	0
76	1 (2.1)	0	1 (2.9)	3 (5.5)
77	2 (4.2)	0	0	2 (3.6)
78	0	0	1 (2.9)	0
79	0	1 (2.6)	0	0

Distribution of chromosome number in WT and Het MMET, early and late stage.

Table S4

Sample	Treatment	Duration of mitosis (min)	Number of cells analyzed
WT/NeuT E	230 nM nocodazole	468±17	65
WT/NeuT E	5 μM nocodazole	652±24	43
WT/NeuT L	230 nM nocodazole	439±11	85
WT/NeuT L	5 μM nocodazole	624±17	106
Het/NeuT E	230 nM nocodazole	493±16	49
Het/NeuT E	5 μM nocodazole	702±14	48
Het/NeuT L	230 nM nocodazole	372±12	50
Het/NeuT L	5 μM nocodazole	481±14	85
WT/NeuT L	10 nM taxol	60 ± 5	79
WT/NeuT L	100 nM taxol	362 ± 43	56
Het/NeuT L	10 nM taxol	37 ± 12	62
Het/NeuT L	100 nM taxol	164 ± 74	91

Duration of mitosis in MMET cells treated in the indicated conditions. Data from time lapse videos reporting timing of cell rounding up (duration of mitosis). Results are shown as mean ± SEM.

Table S5

	Deep Del	Shallow Del	Diploid	Gain	Amp	Total	Somatic Mutation Rate
PIK3C2A	0.1% (1)	22.8% (219)	60.6% (582)	15.7% (151)	0.7 (7)	100% (960)	0.6% (6/960)
PIK3C2B	0% (0)	1% (10)	21.9% (210)	64.3% (618)	12.7% (122)	100% (960)	1.3% (12/960)

Putative copy-number alterations and somatic mutations rate for *PIK3C2A* and *PIK3C2B* (GISTIC) Breast Invasive Carcinoma (TCGA, Provisional). The percentage (%) of patients and their number (n) in each group is indicated.

Variable		All n (% col)	PI3K-C2α low n (% row)	PI3K-C2α high n (% row)	p
All		1779 (100)	857 (48.2)	922 (51.8)	
Age at surgery					<0.001
	<50	722 (40.6)	305 (42.2)	417 (57.8)	
	>=50	1057 (59.4)	552 (52.2)	505 (47.8)	
Histology					<0.001
	Ductal	1457 (81.9)	657 (45.1)	800 (54.9)	
	No Ductal	322 (18.1)	200 (62.1)	122 (37.9)	
pT					0.005
	pT1a/b	161 (9.1)	91 (56.5)	70 (43.5)	
	pT1c	1000 (56.2)	497 (49.7)	503 (50.3)	
	pT2	557 (31.3)	237 (42.5)	320 (57.5)	
	pT3/pT4	61 (3.4)	32 (52.5)	29 (47.5)	
Positive lymph nodes					0.174
	None	843 (47.4)	403 (47.8)	440 (52.2)	
	1+	898 (50.5)	430 (47.9)	468 (52.1)	
	X	38 (2.1)	24 (63.2)	14 (36.8)	
Grade					<0.001
	1	311 (17.5)	195 (62.7)	116 (37.3)	
	2	758 (42.6)	432 (57)	326 (43)	
	3	677 (38.1)	216 (31.9)	461 (68.1)	
	NA	33 (1.9)	14 (42.4)	19 (57.6)	
PVI					0.043
	Absent	1183 (66.5)	590 (49.9)	593 (50.1)	
	Present	596 (33.5)	267 (44.8)	329 (55.2)	
ER					<0.001
	ER=0	291 (16.4)	56 (19.2)	235 (80.8)	
	ER>0	1488 (83.6)	801 (53.8)	687 (46.2)	
ER/PgR					<0.001
	Non expressed (Both 0)	266 (15)	48 (18)	218 (82)	
	Expressed (ER>0 or PgR>0)	1513 (85)	809 (53.5)	704 (46.5)	
HER2 status					<0.001
	NEG	1531 (86.1)	789 (51.5)	742 (48.5)	
	POS	218 (12.3)	53 (24.3)	165 (75.7)	
	NA	30 (1.7)	15 (50)	15 (50)	
Ki-67					<0.001
	<14%	479 (26.9)	293 (61.2)	186 (38.8)	
	>=14%	1299 (73)	564 (43.4)	735 (56.6)	
	NA	1 (0.1)	0 (0)	1 (100)	
Subtype					<0.001
	NA	53 (3)	23 (43.4)	30 (56.6)	
	Luminal	1343 (75.5)	748 (55.7)	595 (44.3)	
	HER2-POS	211 (11.9)	52 (24.6)	159 (75.4)	
	TN	172 (9.7)	34 (19.8)	138 (80.2)	
First Event					---
No event		1258 (70.7)	616 (49)	642 (51)	
Distant Metastasis		243 (13.7)	100 (41.2)	143 (58.8)	
Other events		177 (9.9)	92 (52)	85 (48)	

Association between PI3K-C2α status and the demographic, clinical, and pathological variables (evaluated with chi-sq test). The number (n) of patients and percentage (%) in each group is indicated. Patients were assigned to PI3K-C2α high or low group based on the following scoring systems: IHC, PI3K-C2α low ≤ 1.0, PI3K-C2α high > 1.0. The event Distant Metastasis was defined as the occurrence of distant metastasis or death from breast cancer as a first event. Other events include second primary cancer or death from unknown cause or other cause. pT, primary tumour size; pN, nodal status; PVI, Perivascular invasion; ER: Estrogen receptor; PgR progesterone receptor; Ki-67, proliferation index. Molecular subtypes were defined according to St. Gallen 2013 classification: Luminal, HER2-positive, HER2-POS, Triple-negative, TN. NA, not available. p, p value

Subgroups	Early events Univ. analysis HR (95% CI) high vs. low	p	Multiv. analysis HR (95% CI) high vs. low	p
ALL	1.66 (1.21;2.28)	0.002	1.41 (1.01;1.95)	0.041
Luminal	1.73 (1.17;2.56)	0.006	1.44 (0.97;2.14)	0.072
HER2-POS	0.69 (0.33;1.42)	0.31	0.76 (0.35;1.66)	0.49
TN	1.06 (0.4;2.82)	0.91	1.13 (0.40;3.16)	0.82

Subgroups	Late events Univ. analysis HR (95% CI) high vs. low	p	Multiv.analysis HR (95% CI) high vs .low	p
ALL	0.98 (0.63;1.53)	0.94	0.84 (0.53;1.32)	0.44
Luminal	1.26 (0.79;1.99)	0.33	1.09 (0.68;1.74)	0.72
HER2-POS	1.19 (0.13;10.64)	0.88	1.28 (0.14;11.66)	0.83
TN	NE	---	NE	---

Prognostic value of PI3K-C2α status, as determined by IHC, in subtype subgroups of the IEO BC 97-00 cohort. The hazard ratios (HR) of Distant Metastasis events in the comparison of PI3K-C2α high vs. low tumours were estimated with both univariate and multivariable Cox proportional hazard models with time varying covariate. Multivariable models were adjusted for Grade, Ki-67, HER2 status, estrogen/progesterone status, tumor size, number of positive lymph nodes and age at surgery if available. Patients were assigned to PI3K-C2α high or low group based on the following scoring systems: IHC, PI3K-C2α low ≤ 1.0, PI3K-C2α high > 1.0. Early distant metastasis was define as event occur within 5 years from surgery while Late distant metastasis was define as event occur between 5 and 10 years from surgery. Molecular subtypes were defined according to St. Gallen 2013 classification: Luminal; HER2-positive, HER2–POS; Triple-negative, TN. CI, 95% confidence intervals; p, p value; Ne, not estimable.

Cell line	IC50 (μM)	CI (μM)	LogIC50
MCF7 ctrl	0.018	0.012-0.027	-9,641
MCF7 shPI3K-C2α	0.0002	0.0001-0.0003	-7,739
MCF7 shPI3K-C2α + C2α WT	0.017	0.013-0.027	-7,758
MCF shPI3K-C2α + C2α KD	0.019	0.012-0.031	-7,714
SKBR3 ctrl	0.178	0.1-0.316	-6,749
SKBR3 shPI3K-C2α	0.007	0.004-0.011	-8,177
SKBR shPI3K-C2α +C2α WT	0.170	0.08-0.359	-6,771
SKBR shPI3K-C2α + C2α KD	0.133	0.066-0.266	-6,878
BT474 ctrl	0.104	0.048-0.228	-8,326
BT474 shPI3K-C2α	0.002	0.001-0.004	-8,953
BT474 shPI3K-C2α + C2α WT	0.108	0.054-0.214	-8,631
BT474 shPI3K-C2α + C2α KD	0.108	0.051-0.229	-6,982
MDA231 ctrl	0.169	0.055-0.512	-6,966
MDA231 shPI3K-C2α WT	0.001	0.0004-0.003	-6,968
MDA231 shPI3K-C2α + C2α	0.151	0.044-0.511	-6,773
MDA231 shPI3K-C2α + C2α KD	0.157	0.039-0.623	-8,983
T47D ctrl	0.005	0.003-0.007	-6,822
T47D shPI3K-C2α	0.001	0.0008-0.002	-6,804

Summary of IC50 values, confidence of interval (CI) and LogIC50 measured in response to Paclitaxel for five human breast cancer cell lines after 24h treatment.
Breast cancer cells stably expressing non-target shRNA (scramble) or shPI3K-C2α and an shRNA-resistant WT or KD PI3K-C2α.

Dataset	Regimen	Pathological evaluation	PI3K-C2α Low	PI3K-C2α High	p
Martin et al., 2011	Taxanes				
		pCR	4	1	0.04
		no pCR	14	21	
	Anthracyclines	pCR	3	3	0.5
		no pCR	24	24	
Hatzis et al., 2011	Taxanes and Anthracyclines				
		pCR	55	35	0.02
		no pCR	169	188	

Comparison of pCR rate in PI3K-C2α low and high expressor after Taxane or Anthracycline based neoadjuvant treatment in two independent dataset (n=94 and n=447, respectively). pCR: pathological complete response; P, p value. E-GEOD25066. Association between PI3K-C2α status and pathologic response variables was evaluated with chi-sq test.

Variable	All n (% col)	PI3K-C2α low n (% row)	PI3K-C2α high n (% row)	p
All	43 (100)	12 (27.9)	31 (72.1)	
ER status				ns
ER positive	32 (74.4)	9 (28.1)	23 (71.9)	
ER negative	11 (25.6)	3 (27.3)	8 (72.7)	
HER2 status				0.265
NEG	31 (72.1)	7 (22.6)	24 (77.4)	
POS	12 (27.9)	5 (41.7)	7 (58.3)	
Subtype				0.191
Luminal	32 (74.4)	9 (28.1)	23 (71.9)	
HER2-POS	3 (7)	2 (66.7)	1 (33.3)	
TN	8 (18.6)	1 (12.5)	7 (87.5)	
Pathological Evaluation	6 (14)	5 (83.3)	1 (16.7)	0.004
pCR	6 (14)	5 (83.3)	1 (16.7)	
no PCR	38 (88.4)	7 (18.4)	30 (81.6)	

Baseline characteristics of patients treated with taxane-based chemotherapy (ATx6) in the neoadjuvant settings. pCR: pathological complete response; p, p value.

Acknowledgments

This work was realized thanks to the coordination of Emilio Hirsch and the hard work with Miriam Martini and Federico Gulluni, who shared with me the first authorship of this project. Finally, this work was realized thanks to the collaboration with Carlo Cosimo Campa, Alessandra Ghigo, Jean Piero Margaria, Elisa Ciraolo, Irene Franco, Ugo Ala, Laura Annaratone, Davide Disalvatore, Giovanni Bertalot, Giuseppe Viale, Anna Noatynska, Mara Compagno, Sara Sigismund, Filippo Montemurro, Marcus Thelen, Fan Fan, Patrick Meraldi, Caterina Marchiò, Salvatore Pece, Anna Sapino, Roberto Chiarle, Pier Paolo Di Fiore.

Ringrazio Miriam per avermi guidato durante il dottorato in nome della comune passione per ~~la scienza~~ Harry Potter e nonostante le mie lacune in materia cinematografica (ma alla fine, qual è la differenza tra Guerre Stellari e Star Wars?!).

Ringrazio tutto il gruppo Hirsch/Ghigo/Porporato, in particolare Carlo per il suo supporto, per le sue analisi alternative del genere umano, per la sua passione nel raccontare storie e per aver assecondato la mia dipendenza dal sidro; Ale Ghigo per i suoi saggi consigli, Vale per i mille doppi sensi e le sue meravigliose trippe, Flora per la sua dolcezza e il supporto morale, Jix per la pazienza nel sopportare le mie pignolerie, Polly per i suoi abbracci che mi arrivano al ginocchio, Luca per la sua compassione nel vedermi ad ore tarde in lab, Jeanino per l'adrenalina delle sottomissioni dell'ultimo secondo, Fede per il suo ottimismo e il suo mantra "non ce la faremo mai", Paolo per il tentativo mancato di farmi appassionare al metabolismo, Elisabeth per il ripasso del francese, Myriam per la sua passione per la cucina, Abhi per avermi regalato le "Tutti i gusti +1" che conservo ancora incellofanate, Ming e Kai per aver tentato invano di insegnarmi a mangiare con le bacchette, Roberto per la sua ventata di allegria brasiliana, Marts per le chiacchierate su whatsup e le sue dolci melodie.

Vorrei inoltre ringraziare l'MBC, in particolare Ade per i nostri viaggi e le scarpe consumate, per i suoi giudizi sinceri (fin troppo), per il suo disprezzo per i sacchi che indosso e per le lezioni alla Miccio, Gaia per la sua saggezza e insegnamenti di stile, Sme per sua ilarità e propensione ad essere particolarmente maldestra, Seclì per la condivisione delle pene da reagentariste e mancanza di metanolo, Lorena per la passione condivisa per i musical, la Franca per i suoi consigli sinceri, Orso per le chiacchierate sotto cappa ad ora tarda, il Dottò per la sua follia e i suoi modi di dire romani, Lid per le serate dal vecchio.

Ringrazio Mauretta per le serate torinesi e i revival dei vecchi tempi, Ale per la perseveranza al quizzone, Bottish per la sua pacatezza e razionalità, Vale per avermi trasmesso la passione per i

tessuti, e infine Ile per la sua presenza sempre e comunque, per la sua pazienza per il mio telefono sempre irraggiungibile e per la sua apprensione per la mia vita sregolata.

Un grazie speciale alla mia famiglia, in particolare a mia madre per la sua forza, i suoi insegnamenti e il suo supporto, a mio padre per la sua pazienza, il suo immenso affetto e per la passione condivisa per i documentari e per le sardine, mio fratello per la sua generosità, per la tolleranza delle dosi di assilli e della mancata preparazione sulla formazione della Roma, mia cognata per la sua capacità innata di fare pasticci, per il suo affetto e per le cene di pesce da stelle Michelin, il mio nipotino Amir/Crispi per la gioia infinita che ha portato in famiglia, per essere il mio principino viziato e sulla buona strada per diventare un vero latin lover.